공학박사 학위논문

Generation of Positively Charged Nanobubble and its Applications for Decolorization and Oil-sand Separation

양(+)의 나노기포 생성과 색도 제거 및 기름-모래 분리에서의 적용

February 2020

서울대학교 대학원

건설환경공학부

Bui Thi Thuy

Generation of Positively Charged Nanobubble and its Applications for Decolorization and Oil-sand Separation

지도교수 한 무 영

이 논문을 공학박사 학위논문으로 제출함

2020 년 02월

서울대학교 대학원

건설환경공학부

Bui Thi Thuy

Bui Thi Thuy의 박사 학위논문을 인준함

2020 년 02 월

위 원 장 최 용 주 (인)

부위원장 한 무 영 (인)

위 원 독고 석 (인)

위 원 CHOE JONG KWON (인)

위 원 김 충 일 (인)

Generation of Positively Charged Nanobubble and its Applications for Decolorization and Oil-sand Separation

By

Bui Thi Thuy

Supervisor: Professor Mooyoung Han

A dissertation submitted in partial fulfilment of the requirements

for the degree of

Doctor of Philosophy

Department of Civil and Environmental Engineering

Seoul National University

February 2020

Abstract

Generation of Positively Charged Nanobubble and its Applications for Decolorization and Oil-sand Separation

Bui Thi Thuy

Dept. of Civil and Environmental Engineering

College of Engineering

Seoul National University

Nanobubble (NB) technologies are theoretically and experimentally known to be less chemical consuming and considerable tendency of reducing size of the treatment facility. Hence, they have significant potential for design and operational cost reduction on top of their contribution as an environment friendly technique. With this respect, some feasible applications of the NB technology for water-treatment and particle separation processes are studied

under various conditions and in most of the cases the NB surface charge is one of the major that affects the treatment efficacy. This study therefore focuses on on generation of positively charged nanobubble (NB) in the presence of tri-valent metal ions (especially Al^{3+}) and the applications of such NB for color removal and oil-sand separation. In this research, the NB were produced by dispersing a supersaturated air-water mixture in a mixing chamber, and then causing the breakup of microbubbles in a Teflon hose. The size and zeta potential of the NB were measured by dynamic light scattering. Overall, the NB size had no dependency on pH and grew over time and here, the possible mechanism for the size growth was related to their coalescence in the solutions.

The generation of positively charged NB was observed in the presence of chemical reagents, especially Al^{3+} - the most widely-used coagulant in water treatment. Positive NB generation was confirmed in the presence of the cationic surfactant (dimethyldioctadecylammonium bromide) and was resulted in the addition of tri-valence metal ions (Al^{3+} and Fe^{3+}). The NB zeta potential decreased in all solutions, while their pH increased from 2 to 12. The positively charged NB in the presence of Al^{3+} were created from the specific cationic species (at $pH < 6$) and hydroxide precipitates (at $pH = 6 – 9$) on the NB surface. The effects of Al^{3+} on the behavior of the positive ZP was then observed under conditions: $[Al^{3+}]$ from 0 to 10 mM and timeframe of 150 min.

The results showed that [Al^{3+}] had little effect on the NB size and the NB zeta potential was negatively charged, zero-charged, and positively charged in the addition of [Al^{3+}] of 0, 0.5, and ≥ 1 mM, respectively. Maximum positivity of the ZP was obtained at ~ +20 ± 2 mM when adding ≥ 2 mM Al^{3+}. At all cases, the zeta potential remained over 150 min, confirming the insignificant effects of [Al^{3+}] on the NB stability via the ZP analysis. With these respects, the positive NB in the presence of Al^{3+} were then used to investigate the treatment efficiency for color removal and oil-sand separation.

The experimental results on decolorization proved color reduction of dark green Rit dye using NB in comparison with using Al^{3+} alone and H_2O_2 alone; and showed the role of positive NB, reactive species on decolorization ratio in the processes using NB alone, ultrasonic NB, and NB/H_2O_2. The color removal processes with Al^{3+} alone and H_2O_2 alone were performed using a jar tester while bubbling solutions were injected at a bubble rate of 30% through the bottom of a column reactor containing Rit dye at concentrations of ~500 and ~1200 CU. The results indicated greater color removal for weaker colors at all cases. Furthermore, the decolorization rate using NB systems was more efficient than that using conventional processes. In both dye concentrations, positive ultrasonic NB (ZPs of +15 mV to +20 mV) and positive NB/H_2O_2 (1 mM) systems were found to be effective treatment processes. The color removal mechanisms were owing to the electrostatic attraction between the

positive NB and dye components; furthermore, reactive species such as $OH^{\cdot}$, $HO_2^{\cdot}$, and $O_2^{\cdot}$ were fundamental in enhancing Rit dye degradation in ultrasonic NB and NB/H_2O_2 systems. More than 90% of Rit dye removal was obtained within 30 min and after 60 min in the ultrasonic NB and NB/H_2O_2 systems, respectively. Different decolorization times under various NB presences were attributed to the transfer from the bubbly regime to aggregate regime, and the reaction kinetics of the reactive species and Rit dye components.

In the application for the oil-sand separation, the injection of NB was shown to be an effective treatment process with TPH removal ≥ 85%. The results demonstrated that the NB/oil-sand ratio, separation time, and NB injection (i.e. batch and intermittent regimes) were found to noticeably affect the separation efficiency of the oil-sand by the NB process. The application of the ultrasonic sound was proved to insignificantly improve the separation performance. As resulted, greater TPH removal was obtained with the intermittent injection of positive NB (ZP from +15 to +20 mV) at NB/oil-sand of ≥ 2/1 (v/v), and the separation time from 5 to 20 min. However, negatively charged NB technology can be also considered as a reliable application for the oil-sand separation even it required the greater NB/ oil-sand (ca. ≥ 3/1) and longer treatment time (ca. 40 min). Buoyancy force played the major role on detaching the oil. It was found that the larger external contact angle between bubble and oil layer, the creation of microbubble and macrobubble via NB

coalescence in the oil-sand reactor, and the increase in the number of coalesced bubble attached on the oil layer were fundamental to produce stronger buoyancy force for the better TPH removal.

The NB processes were confirmed to be a reliable evidence for the decolorization of polluted waters and the oil-sand separation. In both fields, the better treatment efficiency was obtained in accordance with the optimal NB zeta potential value of +20 mV; giving the fact that the technology using positive NB formed in the addition of Al^{3+} was the most effective. The findings from this study allow further applications of NB technology as a new horizon for water treatment and soil remediation.

Keyword: Bubble coalescence; bubbles size; bubble zeta potential; dye decolorization; electrostatic attraction; flotation; oil-sand separation; positively charged nanobubble; reactive species

Student number: 2016-37194

Table of Contents

List of Tables

List of Figures

CHAPTER 1. INTRODUCTION

1.1. Background

Recently, nanobubble (NB) have drawn more attention in the field of water treatment and particle separation. A previous work (Agarwal 2011) reported that NB have a role in the catalysis of chemical reactions, used for the purification of contaminated water and the improvement of chemical treatment efficiency. In more details, the performance of NB technology is affected by the physical properties of gas-liquid phases and of contaminants (Tsai 2007, Temesgen 2017). Moreover, the characteristics of NB can be adapted to the chosen design and operational conditions (Najafi 2007, Ushikubo 2010). The size and zeta potential are the major surface properties of bubble, which have been measured under various conditions. A number of studies have focused on the influences of surfactants and/or salt concentration (Saulnier 1996, Kim 2000, Cho 2005, Quinn 2014, Arturo 2015), of frother–electrolyte solutions (Elmahdy 2008, Jose 2011, Castro 2013, Sovechles 2016), paralleled with variations in pH. Recently, (Temesgen 2017) reported that the surface charge of bubbles and contaminants should be opposed to enhance treatment efficiency. In addition, most of the contaminants in the natural water has shown their negative charge (Han 2006), allowing the application of positive bubbles technology for greater surface attraction,

aiming at higher efficacy.

Flotation has been one of the basic separation processes for many decades (Fan 2010). Most of the target substances to be separated by flotation include powders, chemicals, metal ions, oils and organic (Rubio 2002). The need in reduction of bubble size in flotation processes is highly related to improving separation efficiency. (Bui 2015) explained the possibility of optimizing the efficiency of flotation by modification of bubble characteristics mainly size and surface charge in addition to particle properties. From the perspective of flotation, the NB are widely used to remove the contaminants in water with a better efficiency due to its long existence, tailored bubble surface charge, and free radical generation. There is a large body of experimental evidence showing that bubble–particle collection efficiency (Miettinen 2010). Similarly, it was reported the need of bubble size reduction in froth flotation is highly related to increasing the collision probability of small particles with fine gangue. According to the study the probability of colision increases as the bubble size decreases improving the separation efficiency. Surface charge and size of particles as well as small bubbles play an important role in flotation (Bui 2015). The principle for removal mechanism of the contaminants in water is attributed to the similar size and opposite charge between the bubbles and fine particles, which leads to better collision of bubbles and contaminated particles, making it easy to float (Bui 2015).

Several papers have focused on the application of NB to flotation processes: substances like oil, grease, powder, metal ions, and organic matter (Galvin 1994) can be separated from the rest of the solution based on the floatability of bubble-pollutant aggregates (Haarhoff 2001, Tsai 2007, Fan 2010). Increase in concentration of NB in froth flotation increases the stability of NB suspension reducing rising velocity creating favorable condition for froth flotation of coarse particles or hard-to-float particles that require a relatively long slide time (Fan 2010). In another study (Fan 2010) studied the effect of NB on flotation. It has been found that the presence of NB widen flotation particle size range and increased particle surface hydrophobicity and improved froth flotation efficiency. Furthermore, negatively charged NB flotation with coagulation/flocculation process (PAC as coagulant) is concluded as to be a cost-effective treatment for chemical, mechanical polishing of wastewater. The conductivity experiments performed in the lab and the pilot scales conducted by (Tsai 2007) reported an increase of 40% of wastewater clarification efficiency with a good removal of approximately 95% for the turbidity, total solids, and total silica. Moreover, the cost and performance of the NB flotation technology with coagulation/flocculation is found to be considerably lesser than the conventional bubble processes. For a field scale application, the operation needs to be optimized to demonstrate the feasibility of the NB flotation technology.

The NB process can be a potential great application for industrial wastewater, especial textile wastewater. Under the variation of feeding condition in textile factories, the NB would play their role as an efficient treatment technology on decolorizing and reducing turbidity. The NB zeta potential (ZP) (negative or positive) was controlled by adding surfactants/frothers or salts (Temesgen 2017, Bui 2019); thus, the electrostatic attraction would be considered as well as the efficacy of NB–dye molecule aggregates. Adding small amount of strong oxidant is expected to improve the generation of free radicals or reactive species to accelerate the degradation of the dye, as it has been evidenced in microbubble technologies (Quan 2017).

The NB technology is known by their less chemical consuming and considerable tendency of reducing size of the treatment facility. Wide applications of NB for particle separation have been anticipated via the high floatability of the bubble-particle aggregate; making it feasible to be an effective method for the oil remediation from the contaminated sand. Recent works on the oil remediation from the sand have focused on several factors affecting the separation efficiency by bubble technology. (Kim 2012) demonstrated that bubbles with micro size and potential energy (i.e. bursting and collapsing energies) could result in high separation efficiency of the oil-sand. In addition, (Sobhy 2013) proved the improvement in separating hydrophobic particles away from the hydrophilic materials in the application

of the NB. In the oil remediation, the injection of the bubbles with the size from 300 to 400 nm led to enhance the oil flotation efficiency from the sand (Zhou 2010). Finding from these investigations relies on the potential application of the NB in the field of the oil remediation.

1.2. Research Objectives

The main objective of this dissertation are to investigate the application of positively charged nanobubble (NB) for decolorization and oil-sand separation, as followings:

(1) Generate positively charged nanobubble:

   a. Prove generation of positive NB generation in the addition of tri-valence metal ions (Al^{3+} and Fe^{3+}) and propose mechanism for positive NB creation for such cases.

   b. Observe the positive NB behavior in the presence of the most common coagulant (Al^{3+}) at concentrations from 0 ~ 10 mM

(2) Investigate the decolorization of Rit dye using positively charged NB technologies:

   a. Demonstrate a Rit dye color removal in the presence of NB, and

   b. Observe the role of positive NB and reactive species on color removal efficiency.

(3) Investigate the oil-sand separation in the injection of positively charged NB technologies:

a. Observe the bubble coalescence in the oil-sand reactor

b. Evaluate the oil-sand separation efficiency in the injection of NB (expressed by TPH removal), and

c. Observe the effects of the NB operational conditions on the oil-sand separation

1.3. Dissertation structure

This dissertation consists of 6 chapters. Chapter 1 indicates the background, research objectives, and dissertation structure. Chapter 2 presents literature review. Chapter 3 pertains to experimental results for positively charged nanobubble generation in the addition of alum at various concentration and pHs. Chapters 4 focuses on application of positive NB for a Rit dye decolorization. Chapter 5 shows the efficiency of the light oil-sand separation when injecting NB technologies (negatively and positively charged). Chapter 6 summarizes results of this study and suggests possible further research. The structure of this study is shown in Figure 1.1.

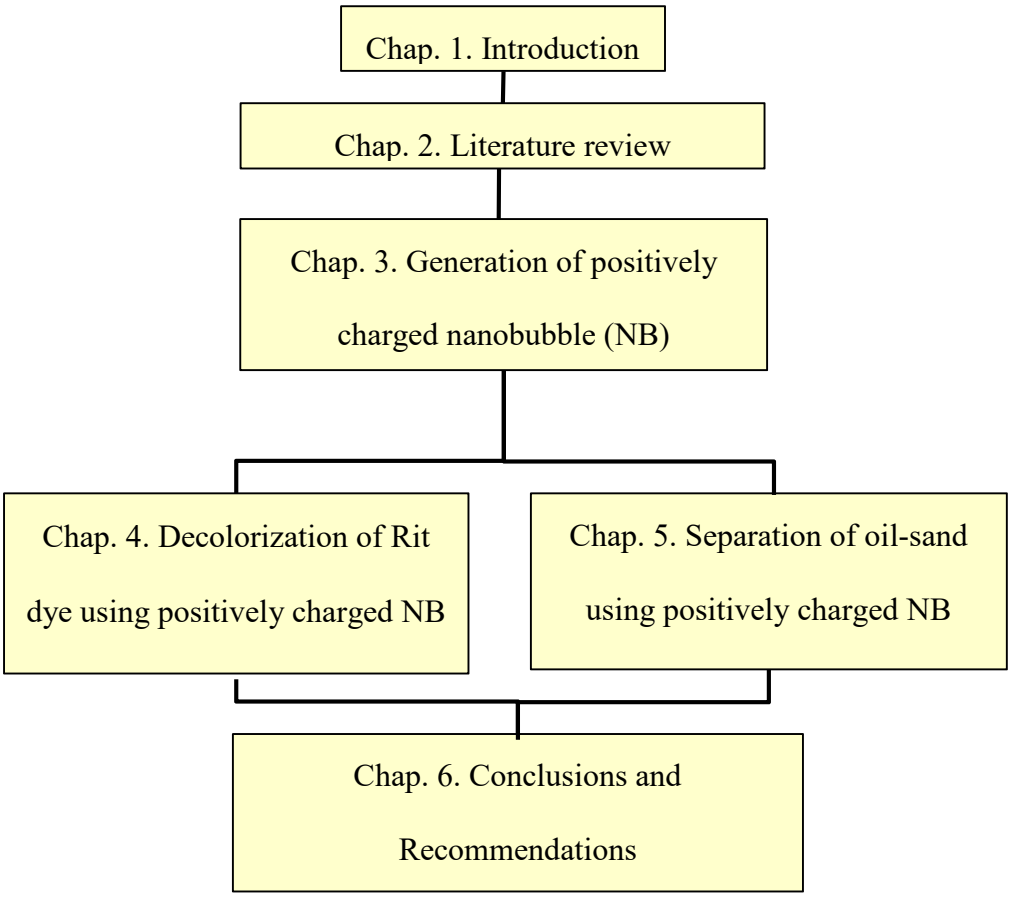

Figure 1.1. Dissertation structure

References

Agarwal, A., W. J. Ng and Y. Liu (2011). "Principle and applications of microbubble and nanobubble technology for water treatment." Chemosphere 84(9): 1175-1180.

Arturo, B.-T., Roberto, P.-G., Diego, M.-C. (2015). "Zeta potential of air bubbles conditioned with typical froth flotation reagents." International Journal of Mineral Processing 140: 50-57.

Bui, T. T. and M. Han (2015). "Removal of Phormidium sp. by positively charged bubble flotation." Minerals Engineering 72: 108-114.

Bui, T. T., S.-N. Nam and M. Han (2015). "Micro-Bubble Flotation of Freshwater Algae: A Comparative Study of Differing Shapes and Sizes." Separation Science and Technology 50(7): 1066-1072.

Castro, S., Miranda, C., Toledo, P., Laskowski, J. S. (2013). "Effect of frothers on bubble coalescence and foaming in electrolyte solutions and seawater." International Journal of Mineral Processing 124: 8-14.

Cho, S.-H., Kim, J.-Y., Chun, J.-H., Kim, J.-D. (2005). "Ultrasonic formation of nanobubble and their zeta-potentials in aqueous electrolyte and surfactant solutions." Colloids and Surfaces A: Physicochemical and Engineering Aspects 269: 28-34.

Elmahdy, A., M., Mirnezami, M., Finch, J., A. (2008). "Zeta potential of air bubbles in presence of frothers." International Journal of Mineral Processing 89: 40-43.

Fan, M., Tao, D., Honake, R., Luo, Z. (2010). "Nanobubble generation and its application in froth flotation (part I): nanobubble generation and its effects on properties of microbubble and millimeter scale bubble solutions." Mining Science and Technology (China) 20(1): 1-19.

Haarhoff, J., Edzwald, J. K. (2001). "Modelling of floc-bubble aggregate rise rates in dissolved air flotation." Water Science and Technology 43(8): 175-184.

Han, M. Y., Kim, M. K., Ahn, H. J. (2006). "Effects of surface charge, micro-bubble size and particle size on removal efficiency of electro-flotation." Water Science and Technology 53(7): 127-132.

Jose, E., B.-A., Sergio, A. B.-R., Raul, G.-G., Alejandro, E.-B., Jose, A. P.-M., Guillermo, G.-A., Jose, L., N.-B. (2011). "Effect of Electrolytes in Aqueous Solution on Bubble Size in Gas-Liquid Bubble Columns." Industrial and Engineering Chemistry Research 50: 12203-12207.

Kim, J., S., Song, M., G., Kim, J., D. (2000). "Zeta Potential of Nanobubble Generated by Ultrasonication in Aqueous Alkyl Polyglycoside Solutions." Journal of Colloid and Interface Science 223(2): 285-291.

Miettinen, T., J. Ralston and D. Fornasiero (2010). "The limits of fine particle flotation." Minerals Engineering 23(5): 420-437.

Najafi, A., S., Drelich, J., Yeung, A., Xu, Z., Masliyah, J. (2007). "A novel method of measuring electrophoretic mobility of gas bubbles." Journal of Colloid and Interface Science 308: 344-350.

Quinn, J., J., Sovechles, J., M., Finch, J., A., Waters, K., E. (2014). "Critical coalescence concentration of inorganic salt solutions." Minerals Engineering 58: 1-6.

Saulnier, P., Lachaise, J., Morel, G., Graciaa, A. (1996). "Zeta Potential of Air Bubbles in Surfactant Solutions." Journal of Colloid and Interface Science 182: 395-399.

Sovechles, J., M., Lepage, M., R., Johnson, B., Waters, K., E. (2016). "Effect of gas rate and impeller speed on bubble size in frother-electrolyte solutions." Minerals Engineering 99: 133-141.

Temesgen, T., Bui, T. T., Han, M. Y., Kim, T.-I., Park, H. J. (2017). "Micro and nanobubble technologies as a new horizon for water-treatment techniques: A review." Advances in Colloid and Interface Science 246: 40-51.

Tsai, J., C., Kumar, M., Chen, S.-J., Lin, J.-G. (2007). "Nano-bubble flotation technology with coagulation process for the cost-effective treatment of chemical mechanical polishing wastewater." Separation and Purification

Technology 58: 61-67.

Ushikubo, F., Y., Furukawa, T., Nakagawa, R., Enari, M., Makino, Y., Kawagoe, Y., Shiina, T., Oshita, S. (2010). "Evidence of the existence and the stability of nano-bubbles in water." Colloids and Surfaces A: Physicochemical and Engineering Aspects 361: 31-37.

CHAPTER 2. LITERATURE REVIEWS

2.1. Overview on nanobubble (NB)

The presence and stability of NB has been a controversial issue since the proposal of their contribution to the attraction between hydrophobic surfaces in water (Berkelaar 2013, Walczyk 2014). Since then, many researchers investigated their presence using different techniques (Ushikubo 2010, Walczyk 2014). Similar to the case of the microbubbles, the researchers did not arrive at a consensus regarding the definition of the NB; moreover, some of the definitions exclude a range of bubble sizes that is not between the minimum size proposed for the MBs and the maximum for the NB. Agarwal 2011 did not classify the bubbles that fall in the range between 200 nm and 10 μm. Based on their definition, the diameters below 200 nm represent the NB. To define this range, Agarwal 2011 presented the names 'micro-nano bubbles' (MNB) based on the suggestion from (Tsuge 2010), which shows the confusion and lack of a clear category for ultrafine bubbles. In addition, Wu 2012 defined the NB or sub-micron bubbles as bubbles having sizes less than a micron and categorized the bubbles they generated with a size less than 500 nm as sub-MBs or NB. Moreover, Parmar 2013 recently defined the NB as bubbles having a diameter less than few hundreds of a nanometer, which is vague and controversial. By summarizing the upper limit of the bubbles that

different researchers considered for NB, bubbles less than a micron was found reasonable to categorize them under ultrafine bubbles/NB based on their measured size and shared similarity of properties, as shown in Figure 2.1.

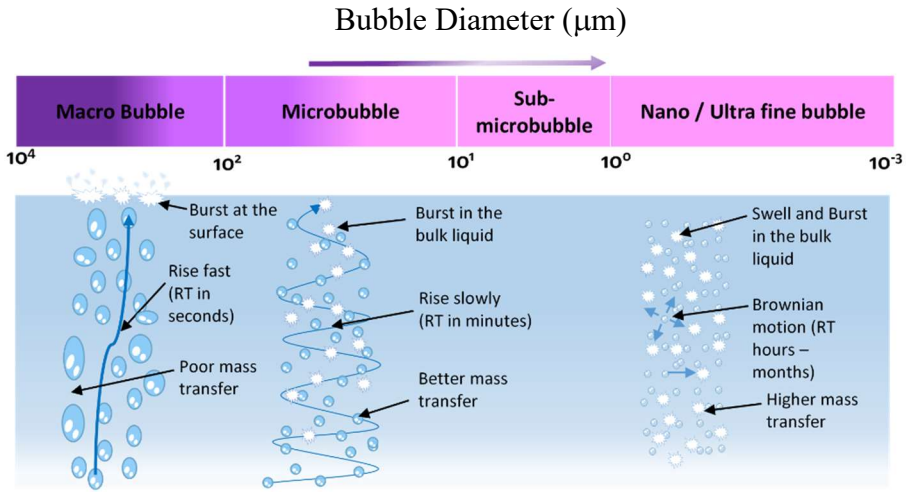

Figure 2.1. Proposed range of the bubble sizes and major properties (source: Temesgen 2017)

Basically, bubbles are formed through coalescence and breakup, which are two opposite mechanisms (Agarwal 2011). In coalescence mechanism, fine bubbles contact to grow their size and breakup mechanism results in the formation of ultrafine (nano) bubbles. Different studies applied different techniques of ultrafine bubble generation: hydrodynamic cavitation and particle cavitation (Agarwal 2011), acoustic or sonication (Xu 2008, Kim 2010, Agarwal 2011), electrochemical cavitation (Wu 2008), and mechanical agitation (Xu 2008).

2.2. Physical properties of the NB

2.2.1. NB size

The size of NB is measured by using laser-diffraction particle-size analyzer (Yoshida 2001, Yoshida, Masuda 2003, Cho 2005, Kukizaki 2006, Takahashi 2007, Han 2009, Tasaki 2009, Agarwal 2011, Xiong 2015). Laser-diffraction particle-size analyzer is a simple tool that can be used to obtain the average size of a large number of bubbles without a visible image. It employs bubble size measurement technique based on their light-scattering properties. It is applicable to measure sizes ranging from approximately 0.1μm to 3 mm. (Kobayashi 2014) proposed another technique for determination of ultrafine bubbles using resonant mass measurement method. It is assumed to solve the drawbacks of other conventional techniques in differentiating particles from NB with the size range of 100-200 nm. It is capable of distinguishing positively buoyant particles (bubbles) from negatively buoyant particles. Because the NB exist in water for a considerable duration of time, along with its stability (Ushikubo 2010), the need of a simple and field adaptive method is highly needed.

For the case of the NB, the pressure (Kim 2012, Kim 2014), sonic power (Cho 2005) – as provided in Table 2.1, and other operation conditions, such as the length, diameter, and type of hose (Kim 2010) are introduced as

relatively major factors affecting the size. (Ushikubo 2010) indicated that different types of gases used in bubble creation; such as oxygen and air, resulted in NB with similar, common average sizes (measured using particle analyzer) of 137 nm and 140 nm, respectively. In addition, Ohgaki 2010 reported that the NB diameter had no dependence on the use of N_2, CH_4, and Ar; with the average size of ~ 100 nm.

Table 2.1. Average size of the NB under sonic power (Cho 2005)

Sonic power (W)	50	100	150	200
NB size (nm)	750	935	921	965

In frother-electrolyte solutions, i.e. NaCl and synthesis sea salt solution (containing NaCl and other salt ions), along with frother addition of a flotation cell, influence of the air flow rate and impeller speed – two main operation variables on relatively large MBs size have been carried out (O'connor 1990, Castro 2013, Sovechles 2016). As results, at a lower impeller speed of 4.2 m/s or a higher gas velocity of 0.5 cm/s under some operating conditions, bubble size of the synthesis sea salt solution is about of 850 μm, higher than all of the synthesis salt/frother solutions (~ 650 – 700 μm) (Sovechles 2016), supporting the discussion on the reduction of bubble size due to an addition of frother to the sea water solution (Castro 2013, Laskowski 2003, Quinn 2014).

Furthermore, a comprehensive study of a single impeller speed and gas flow rate was conducted for a detailed explanation on the interaction between frothers and salts. (Sovechles 2016) concluded that in the absence of frother (i.e. Methyl isobutyl carbinol – MIBC), bubbles formed in the 0.5 M NaCl and synthesis sea salt solution were smaller than in deionized water. The study also provided the range of frother concentration added into the solution. It was found that by adding small amount of frother (as 1 – 10 ppm of MIBC), bubble created in 0.5 M NaCl solution overall increased its size in comparison with in a frotherless NaCl solution. And at above 10 ppm of MIBC, all electrolyte solutions produced bubbles with similar size. More results on difference in bubble size of each solution in the presence of frother are shown in table 2.

Table 2.2. Bubble size of the frother-electrolyte solutions at different concentration**

Average bubble size (μm)	Frother (MIBC) concentration (ppm)										
	0	1	2	3	4	5	6	10	15	20	50
Deionized water	3700	2800	2500	2300	2200	1800	1450	1000	900	900	850
0.5 M NaCl	750	760	800	800	780	800	850	1000	900	900	850
Sea salt solution	1200	950	850	850	800	850	850	870	900	900	900

** adopted from (Quinn 2014, Sovechles 2015, Sovechles 2016)

To discuss the differences in the case of frother absence, ionic strength of electrolyte solution which related to critical coalescence concentration was attributed (O'connor 1990, Castro 2013, Sovechles 2015, Sovechles 2016). The synthesis sea salt solution with the ionic strength of 0.7 produced larger bubbles compared to NaCl solution with the ionic strength of 0.5. Also, (Sovechles 2015) summanized that the critical coalescence concentration would be extended to saline solutions with the solution's ionic strength has an ability to reduce bubble size. When comparing the synthesis sea salt solution and NaCl solution, (Sovechles 2016) indicated the interactions of the salt ions presented in synthesis sea salt solution, being the cause of the larger bubble size. Regarding to this, many researches had been conducted, considering NaCl solution as a base and other salt ions (i.e. $MgCl_2$, $CaSO_4$, $MgSO_4$, and KCl) independently added in order to investigate their effect on formed bubble size. As resulted, 0.5 M NaCl created the smallest bubble in the absence of the frother while the addition of $MgCl_2$, $CaSO_4$, and KCl to NaCl had an insignificance on the bubble sized difference; and in contrast, a mixtures of frotherless $MgSO_4$ and NaCl generated larger bubbles (Quinn 2014, Sovechles 2015, Sovechles 2016). In this perspective, the authors attributed to the effects of Mg^{2+} and SO_4^{2-} on bubble coalescence. It was also assumed that at 0.5 M NaCl, the coalescence inhibition had been maximized and the changes in bubble size could be due to the break-up phenomena (Quinn 2014, Sovechles

2015). This breakage has a relevance to the local stress on the surface of the air/water interface when frother is added into the solution (Chu 2016, Sovechles 2016). The role of frother in bubble break-up with a proposed mechanism of inducing surface tension gradient to increase the instability between air and water interface was summarized by (Chu 2016). The conclusion of the effect of the frother on the coalescence and break-up demonstrated the difference in bubble size of frother-electrolyte solution.

2.2.2. Zeta potential of NB

2.2.2.1. Principle of measurement

A fundamental zeta-potential calculation method for the NB is the application of the Smulochowski's equation (Dockko 1998, Spanos 1999, Yang 2001, Han 2004, Cho 2005, Takahashi 2005, Ushikubo 2010, Kim 2014). In many studies, zeta potential analyzers (such as zetaphoremeter III–Shephy, France; zetaplus–Brookhaven Instruments Co., New York; zeta potential analyzer–Zeecom MicroTech Co. Ltd, Japan, etc.) are widely used (Cho 2005, Ushikubo 2010, Kim 2014). This system detects the electrophoretic mobility (horizontal speed in the recorded image) of the bubble at the stationary plane in the measurement cell, and the zeta potential is then calculated from the recorded speed. In addition, in many cases, an electrophoretic system that have an electrophoretic cell (measurement cell), a

video camera, and a video image analysis software is applied to measure the value of the zeta potential (Bui 2015 a, b), as shown in Figure 2.2.

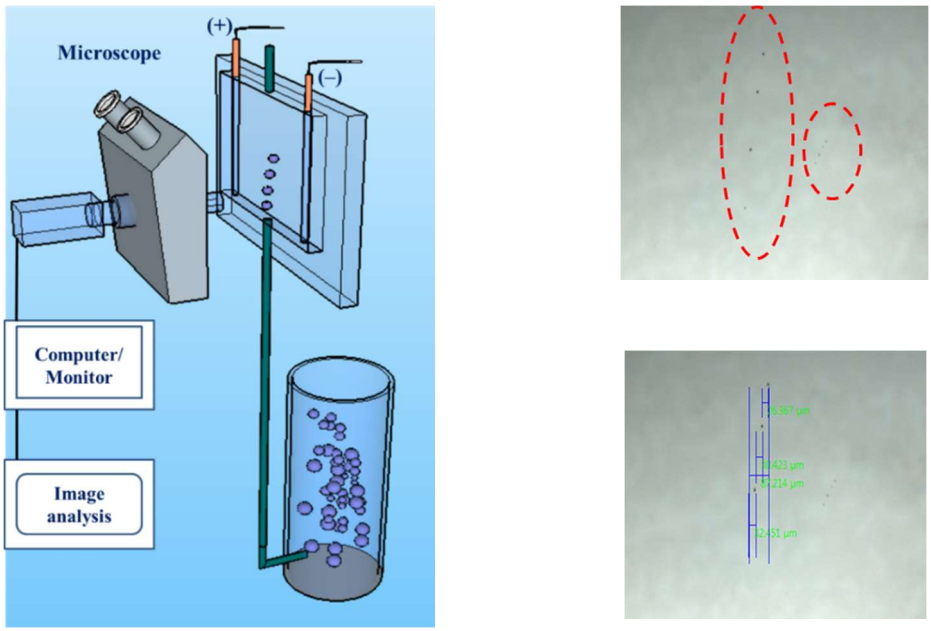

a b

Figure 2.2. Measurement system of the zeta potential and the images of a single bubble captured in the electrolyte solution with respect to time (adopted from Bui, 2015)

2.2.2.2. Zeta potential of NB in surfactant solution

Overall, zeta potential of bubble is a function of electrolyte properties and chemical surfactants of the solution under various pH (Cho 2005, Elmahdy 2008, Bueno-Tokunaga 2015). Similar to microbubbles, the NB are negatively charged in the pH range of 2–12 in a background solution of 0.01 M NaCl or

KCl. At a neutral pH, the negativity of the zeta potential are shown in several studies, with approximately -50 mV (Okada 1990), approximately -40 mV (Cho 2005). The negativities of the NB are related to OH^- ions adsorption to the interface of the bubbles from the background electrolyte. The mechanism that induces selective adsorption of OH^- ions is a combination of the water molecular dipole orientation at the surface and structural differences between water surrounding surface and in the bulk (Karraker 2002). For divalent coagulant additions, such as Mg^{2+} and Ca^{2+}, the zeta potential of the MBs yielded negative results, varying from approximately -45 to -20 mV (Figure 2.3) (Yang 2001, Han 2004).

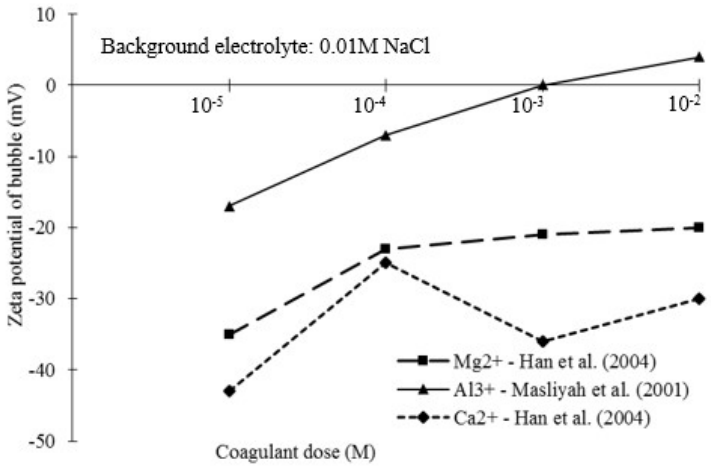

Figure 2.3. Zeta potential of MBs and NB in the presence of various coagulants (a - adopted from Yang 2001 and Han 2004)

In literatures, the electro-kinetic properties of interface which affects

bubble zeta potential could be modified, based on the adsorption of anions (OH-) and/or desorption of cations (H^+) (Takahashi 2005). Regarding to this, the researchers focused on the certain flotation collector, primary amines, and fatty acids. In addition, (Saulnier 1996) investigated the response of cationic surfactant (i.e. tetradecyltrimethylammonium bromide (TTAB, Fluka, purity higher than 98%)), anionic surfactant (i.e. hexadecylbenzenesulfonate), and nonionic surfactants (i.e. decaoxyethylene octylphenol (EO10OP, Gaf) and ethylene dodecanol (EO6DD, Nikko) on changing zeta potential of air bubble under pH from 5 to 8. Furthermore, Najafi 2007 and Kim 2000 have indicated that the charge on the NB depends on the surfactant solution and its ionization properties at different pH values. Surfactants which are categorized to the cationic (i.e. cetyltrimethylammonium bromide – CTAB and/or dodecylamine hydrochloride – DAH), anionic (i.e. sodium dodecyl sulfate – SDS), and non-ionic (as pure water and/or alkyl polyglycoside- AG) groups are well-applied in both MBs and NB technology to provide an implication on properties of air-water interface, affecting zeta potential of bubble. Cationic surfactants as CTAB and/or DAH can change the electrical charge of the inner surface and adsorb onto bubble surface, produce a positive electrical charge. It was abstracted that the charge on the NB was positive in CTAB (Kim 2000) and DAH at pH < 12 (Najafi 2007). Saulnier 1996 has mentioned the reflection of the anionic surfactant on the negativity of microspheres' electrophoretic

mobility due to the adsorption ability of the negative groups of anionic molecules on the microspheres. Following this research, some of contributions on surface charge of the NB have been performed, showing the negatively charged for all pH values in pure water, AG (Kim 2000), and SDS solutions (Kim 2000, Najafi 2007). In summary, Table 2.2 gives the dependency of the surface charge of the NB on the surfactant solutions. In conclusion, the possibility of the adsorption and surface ionization of surfactants on MBs and NB surface are the typical mechanism related to the shifting of zeta potential (Cho 2005, Elmahdy 2008, Kim 2000). The results, cationic surfactant produces positive bubble meanwhile anionic and non-ionic surfactant apply a negative charge to the surface of bubble (Kim 2000, Cho 2005, Elmahdy 2008).

Table 2.3. Average zeta potential of the NB (mV) in different surfactant solutions at various pH

pH	SDS[a, b]	AG[b]	Pure water[a]	CTAB[b]	DAH[a]
2	~ -39	N/A	N/A	N/A	~ +70
3	~ -60	~ -1.30	-0.27	~ +47	~ +50

4	~ -55	N/A	N/A	N/A	~ +58
5.5	~ -64	N/A	~ -4.21	N/A	~ + 49
7	~ -70	~ 8.12	~ -15.68	~ +43	~ +54
11	N/A	N/A	~ -26.73	~ +39	~ +5
12	~ -73	~ -26.86	N/A	~ +38	~ -9

[a] Adopted from (Najafi 2007)

[b] Adopted from (Kim 2000)

2.3. Bubble technology for decolorization and oil-sand separation

2.3.1. Decolorization

Currently, dye wastewater from textile and dye industries has become a significant challenge in wastewater treatment. A dye contaminant, that indicates color to the water, is addressed as an important environmental concern (Yıldırım 2011). In an estimation, about 10 – 15% of the synthesis dye has been discharged in wastewaters (Daneshvar 2008). As the trend of dazzle to natural fabric and synthetics has emerged recently, all-purpose Rit dyes are widely used to color garments, household items, etc., thus releasing strong color pollutants into water bodies. The color of dyes have been reported to cause adverse effects on the environment and human health (Fan 2014, Cardoso 2016). Removal of color from the dyes has been essential in recent decades (Zhao 2018).

So far, numerous decolorization processes have been applied to dye-containing wastewater, such as physical, chemical, and biological treatments (Pandey 2007). In physical treatments, adsorption is effective on transferring dyes from waters to the adsorbents and the dyes has not been degraded (Zhao 2018). Although many conventional chemical methods that are rely on the treatability of coagulants (Ramavandi 2014) are efficient, they usually require high concentration of chemicals and time-consuming. Application of

biological methods are known to be economical; however, the efficacy is depended on the activity of bacteria and it is not feasible to biodegrade the toxic dyes at low concentration (Jha 2016, Cao 2017).

To dates, advanced oxidation processes (AOPs) have been well-applied in textile wastewater treatment (Kumara 2009, Moissa 2018, Kang 2019). Many AOPs, including ozonation (Konsowa 2009, Yıldırım 2011, Fan 2014, Cardoso 2016, Quan 2017), photocatalysis and photoelectrocatalysis (Yıldırım 2011, Cardoso 2016), Fenton reactions (de Lunaa 2013, Muslim. M. 2013, Cai 2016), H_2O_2 and H_2O_2-based processes (Basturk 2015, Moissa 2018, Paz 2018, Pang 2019), ultrasound (Zhao 2018), and bubble column (Konsowa 2009, Turhan 2013), have shown the great performance on decolorizing the dye wastewaters. Bubble technologies, primarily known as adsorptive bubble separation, have been recently studied as an AOP for color wastewater treatment. This process reduces color by attaching dye components and creating a floatable layer through buoyancy force (Kumara 2009, Cai 2016). In many studies, ozone microbubbles, owing to their strong oxidation capacity and nontoxic breakdown products, are formed to enhance decolorization removals (Konsowa 2009, Quan 2017); however, to complete decolorization within the retention time of the microbubbles (several minutes), a relatively high concentration of ozone is required, i.e., ~ 75 g/L (Quan 2017). A similar trend of adding more oxidant chemicals, such as H_2O_2 and Fe^0/H_2O_2

in a microbubble reactor for better color removal, has been reported by (Kumara 2009, Cai 2016). To reduce chemical dose during color treatment, bubbles should be well-retained in the solution to improve bubble–dye molecule attachment.

NB have attracted attention because of their unique characteristics such as high mass transfer, OH· generation, and stable existence (Temesgen 2017). The NB zeta potential (ZP) (negative or positive) was controlled by adding surfactants/frothers or salts (Temesgen 2017, Bui 2019); thus, the electrostatic attraction would be considered as well as the efficacy of NB–dye molecule aggregates. Adding small amount of strong oxidant is expected to generate free radicals or reactive species to accelerate the degradation of the dye, as it has been evidenced in microbubble technologies (Quan 2017). To allow the application NB technologies for dye waters, it can be useful to study the decolorization mechanism of several factors.

2.3.2. Oil removal

Crude oil spills that occur in the rigs, pipeline, onshore and offshore, storage tank, and tanker have contaminated the soil/sand (Lim 2015, Chen 2018); causing severe impacts to the environment and human health (Aguilera 2010). In the event of the oil-sand, the oil trends to adhere to the sand through the adsorption and inhalation mechanisms (Wang 2009, Vijayaraghavan

2019); making it challenging to be cleaned up. In this respect, the application of the efficient technologies to facilitate the oil removal from the contaminated sand should be adopted as a major environmental concern. Many studies have been focused on separation of the oil-sand. Although the common applied technologies, i.e. pressurized washing water (Peters 2018), chemical treatment with surfactant (Ahmadi 2013), and biological remediation (Zheng 2012), have proved to be efficient separation processes, they are generally operated with the high retention time. Feasible techniques for oil detachment should be used to reduce the treatment time.

Bubble technology is an enable technique for separation of the oil from the contaminated soil/sand (Li 2013, Lim 2016). The effectiveness of the bubble technology depends on the interaction between bubbles and the oil layer (Owens 2003) in accordance with two typical mechanisms, i.e. the formation of bubble-oil aggregates when bubbles attach to the oil and the detachment of the bubble-oil aggregates due to flotation of the bubbles (Kim 2012). The increase in the bubble-oil attachment that is influenced by bubble physical properties leads to improve the separation performance of the oil-sand by bubble technology (Lim 2016). Finding from these investigations relies on the potential application of the NB in the field of the oil remediation. To demonstrate the efficiency of the NB process for oil-sand separation, it is good to study the effects of the operational conditions.

References

Agarwal, A., W. J. Ng and Y. Liu (2011). "Principle and applications of microbubble and nanobubble technology for water treatment." Chemosphere 84(9): 1175-1180.

Ahmadi, M., A., Shadizadeh, S., R. (2013). "Implementation of a high-performance surfactant for enhanced oil recovery from carbonate reservoirs." Journal of Petroleum Science and Engineering 110: 66-73.

Basturk, E., Karatas, M. (2015). "Decolorization of antraquinone dye Reactive Blue 181 solution by UV/H2O2 process." Journal of Photochemistry and Photobiology A: Chemistry 299: 67-72.

Bueno-Tokunaga, A., Pérez-Garibay, R., Matinez-Carrillo, D. (2015). "Zeta potential of air bubbles conditioned with typical froth flotation reagents." International Journal of Mineral Processing 140: 50-57.

Bui, T. T. and M. Han (2015). "Removal of Phormidium sp. by positively charged bubble flotation." Minerals Engineering 72: 108-114.

Bui, T. T., S.-N. Nam and M. Han (2015). "Micro-Bubble Flotation of Freshwater Algae: A Comparative Study of Differing Shapes and Sizes." Separation Science and Technology 50(7): 1066-1072.

Bui, T., T., Nguyen, D., C., Han, M., Y. (2019). "Average size and zeta

potential of nanobubble in different reagent solutions." Journal of Nanoparticle Research 21(8).

Cai, M., Su, J., Zhua, Y., Wei, X., Jin, M., Zhang, H., Dong, C., Wei., Z. (2016). "Decolorization of azo dyes Orange G using hydrodynamic cavitation coupled with heterogeneous Fenton process." Ultrasonics Sonochemistry 28: 302-310.

Cao, Z., Zhang, J., Zhang, J., Zhang, H. (2017). "Degradation pathway and mechanism of reactive brilliant Red X–3B in electro–assisted microbial system under anaerobic condition." Journal of Hazardous Materials 329: 159-165.

Cardoso, C., Bessegato, G., Zanoni, M. (2016). "Efficiency comparison of ozonation, photolysis, photocatalysis and photoelectrocatalysis methods in real textile wastewater." Water Reasearch 98: 39-46.

Chen, J., Zhang, W., Li, S., Zhang, F., Zhu, Y., Huang, X. (2018). "Identifying critical factors of oil spill in the tanker shipping industry worldwide." Journal of Cleaner Production 180: 1-10.

Cho, S., H., Kim, J., Y., Chun, J., H., Kim, J., D. (2005). "Ultrasonic formation of Nanobubble and their zeta-potential in aqueous electrolyte and surfactant solutions." Colloids and Surfaces A: Physicochemical and Engineering Aspects 269: 28-34.

Chu, P., Waters, K., E., Finch, J., A. (2016). "Break-up in formation of small bubbles: break-up in a confined volume." Colloids and Surfaces A: Physicochemical and Engineering Aspects 503: 88-93.

de Lunaa, M., D., G., Coladesa, J., I., Sub, C., C., Lu, M., C. (2013). "Comparison of dimethyl sulfoxide degradation by different Fentonprocesses." Chemical Engineering Journal 232: 418-424.

Ebina, K., K. Shi, M. Hirao, J. Hashimoto, Y. Kawato, S. Kaneshiro, T. Morimoto, K. Koizumi and H. Yoshikawa (2013). "Oxygen and Air Nanobubble Water Solution Promote the Growth of Plants, Fishes, and Mice." PLoS ONE 8(6): e65339.

El-Zahaby, A. M. and A. S. El-Gendy (2016). "Passive aeration of wastewater treated by an anaerobic process—A design approach." Journal of Environmental Chemical Engineering 4(4, Part A): 4565-4573.

Fan, M., D. Tao, R. Honaker and Z. Luo (2010). "Nanobubble generation and its application in froth flotation (part I): nanobubble generation and its effects on properties of microbubble and millimeter scale bubble solutions." Mining Science and Technology (China) 20(1): 1-19.

Fan, M., D. Tao, R. Honaker and Z. Luo (2010). "Nanobubble generation and its applications in froth flotation (part II): fundamental study and theoretical analysis." Mining Science and Technology (China) 20(2): 159-177.

Fan, X., Restivo, J., Orfao, J., M., Fernando, M., Pereira, R., Lapkin, A., A. (2014). "The role of multiwalled carbon nanotubes (MWCNTs) in the catalytic ozonation of atrazine." Chemical Engineering Journal 241: 66-76.

Jyoti, K. K. and A. B. Pandit (2001). "Water disinfection by acoustic and hydrodynamic cavitation." Biochemical Engineering Journal 7(3): 201-212.

Jyoti, K. K. and A. B. Pandit (2003). "Hybrid cavitation methods for water disinfection: simultaneous use of chemicals with cavitation." Ultrasonics Sonochemistry 10(4–5): 255-264.

Kang, Y., G., Yoon, H., W., Lee, C., S., Kim, E., J., Chang, Y., S. (2019). "Advanced oxidation and adsorption bubble separation of dye using MnO2-coated Fe3O4 nanocomposite." Water Reasearch 151: 413-422.

Kim, J. Y. S., M.-G. Song and J.-D. Kim (2000). "Zeta Potential of Nanobubble Generated by Ultrasonication in Aqueous Alkyl Polyglycoside Solutions." Journal of Colloid and Interface Science 223(2): 285-291.

Kim, J.-H., Von G. U., Martin B. J. (2004). "Simultaneous Prediction of Cryptosporidium parvum Oocyst Inactivation and Bromate Formation during Ozonation of Synthetic Waters." Environmental Science and Technology 38: 2232-2241.

Kim, T. I., Y. H. Kim and M. Han (2012). "Development of novel oil washing process using bubble potential energy." Marine Pollution Bulletin 64(11):

2325-2332.

Kobayashi, H., S. Maeda, M. Kashiwa and T. Fujita (2014). Measurement and identification of ultrafine bubbles by resonant mass measurement method.

Konsowa, A., H. (2009). "Decolorization of wastewater containing direct dye by ozonation in a batch bubble column reactor." Desalination 158: 233-240.

Kumara, M., S., Sonawanea, S., H., Pandit, A., B. (2009). "Degradation of methylene blue dye in aqueous solution using hydrodynamic cavitation based hybrid advanced oxidation processes." Chemical Engineering & Processing: Process Intensification 122: 288-295.

Li, H., Chow, R., Roberge, K. (2013). "Role of carrier flotation in accelerating bitumen extraction recovery from mineable athabasca oil-sands." The Canadian Journal of Chemical Engineering 91(8): 1340-1348.

Li, H., Hu, L., Song, D., Al-Tabbaa, A. (2014). "Subsurface Transport Behavior of Micro-Nano Bubbles and Potential Applications for Groundwater Remediation." International Journal of Environmental Research and Public Health 11(1): 473.

Lim, M., W., Lau, E., V., Poh, P., E. (2016). "A comprehensive guide of remediation technologies for oil contaminated soil—present works and future directions." Marine Pollution Bulletin 109(1): 14-45.

Lim, M., W., Lau, E., V., Poh, P., E. (2016). "Analysis of attachment process of bubbles to high-density oil: Influence of bubble size and water chemistry." Journal of the Taiwan Institute of Chemical Engineers 68: 192-200.

Lim, M., W., Lau, E., V., Poh, P., E., Chong, W., T. (2015). "Interaction studies between high-density oil and sand particles in oil flotation technology." Journal of Petroleum Science and Engineering 131: 114-121.

Linek, V., M. Kordač and T. Moucha (2005). "Mechanism of mass transfer from bubbles in dispersions: Part II: Mass transfer coefficients in stirred gas–liquid reactor and bubble column." Chemical Engineering and Processing: Process Intensification 44(1): 121-130.

Mezule, L., Tsyfansky, S., Yakushevich, V., Juhna, T. (2009). "A simple technique for water disinfection with hydrodynamic cavitation: Effect on survival of Escherichia coli." Desalination 248(1–3): 152-159.

Moissa, F., L., Mittersteiner, M., Saugo, R., Floriani, T., C., de Jesus, P., C. (2018). "Kinetic behavior of C.I. Reactive Blue 182 towards oxidation with H2O2/UV and H2O2/NaOH systems." Journal of Molecular Liquids 264: 675-682.

Muslim. M., H., M., A., Islam, T., S., A., Ismail, I., M., I., Mahmoo, A., J. (2013). "Decolorization of Diazo Dye Ponceau S by Fenton Process."

Pandey, A., Singh, P., Lyengar, L. (2007). "Bacterial decolorization and

degradation of azo dyes." International Biodeterioration & Biodegradation 59: 73-84.

Pang, J., Fu, F., Li, W., Zhu, L., Tang, B. (2019). "Fe-Mn binary oxide decorated diatomite for rapid decolorization of methylene blue with H2O2." Applied Surface Science 478: 54-61.

Paz, E., C., Aveiro, L., R., Pinheuro, V., S., Souza, F., M., Silva, F., L., Hammer, P., Lanza, P., R., V., Santos, M., C. (2018). "Evaluation of H2O2 electrogeneration and decolorization of Orange II azo dye using tungsten oxide nanoparticle-modified carbon." Applied Catalysis B: Environmental 232: 436-445.

Peters, C., A., Hallmann, C., George, S., C. (2018). "Phenolic compounds in oil-bearing fluid inclusions: Implications for water-washing and oil migration." Organic Geochemistryjournal 118: 36-46.

Prince, M. J. and H. W. Blanch (1990). "Bubble coalescence and break-up in air-sparged bubble columns." AIChE Journal 36(10): 1485-1499.

Quan, X., Luo, D., Wu, J., Li, R., Cheng, W., Ge, S. (2017). "Ozonation of acid red 18 wastewater using O3/Ca(OH)2 system in a micro bubble gas-liquid reactor." Journal of Environmental Chemical Engineering 5(1): 283-291.

Quinn, J., J., Sovechles, J., M., Finch, J., A., Waters, K., E. (2014). "Critical coalesence concentration of inorganic salt solution." Minerals Engineering 58:

1-6.

Ramavandi, B., Farjadfard, S. (2014). "Removal of chemical oxygen demand from textile wastewater using a natural coagulant." Korean Journal of Chemical Engineering 31(1): 81-87.

Sobhy, A., Tao, D. (2013). "High-efficiency nanobubble coal flotation." International Journal of Coal Preparation and Utilization 33(5): 242-256.

Sovechles, J., M., Waters, K., E. (2015). "Effect of ionic strength on bubble coalescence in inorganic salt and seawater solutions." AlChE Journal 61(8): 2489-2496.

Takahashi, M. (2009). "Base and technological application of micro-bubble and nanobubble." Material Integration 22: 2-19.

Temesgen, T., Bui, T. T., Han, M. Y., Kim, T.-I., Park, H. J. (2017). "Micro and nanobubble technologies as a new horizon for water-treatment techniques: A review." Advances in Colloid and Interface Science 246: 40-51.

Tsai, J.-C., M. Kumar, S.-Y. Chen and J.-G. Lin (2007). "Nano-bubble flotation technology with coagulation process for the cost-effective treatment of chemical mechanical polishing wastewater." Separation and Purification Technology 58(1): 61-67.

Tsuge, H. (2010). "Fundamentals of microbubbles and Nanobubble." Bulletin

of the society of sea water science 64: 4-10.

Turhan, K., Ozturkcan, S., A. (2013). "Decolorization and Degradation of Reactive Dye in AqueousSolution by Ozonation in a Semi-batch Bubble Column Reactor." Water Air and Soil Pollution 224(1): 1-13.

Ushikubo, F. Y., T. Furukawa, R. Nakagawa, M. Enari, Y. Makino, Y. Kawagoe, T. Shiina and S. Oshita (2010). "Evidence of the existence and the stability of nano-bubbles in water." Colloids and Surfaces A: Physicochemical and Engineering Aspects 361(1–3): 31-37.

Vijayaraghavan, V., Lau, E., V., Goyal, A., Niu, X., D., Garg, A., Gao, L. (2019). "Design of explicit models for predicting the efficiency of heavy oil-sanddetachment process by flotation technology." Measurement 137: 122-129.

Walczyk, W. and H. Schönherr (2014). "Characterization of the Interaction between AFM Tips and Surface Nanobubble." Langmuir 30(24): 7112-7126.

Wang, J., Yin, J., Ge, L., Zheng, J. (2009). "Using flotation to separate oil spill contaminated beach sands." Journal of Environmental Engineering 136(1): 147–151.

Wu, C., K. Nesset, J. Masliyah and Z. Xu (2012). "Generation and characterization of submicron size bubbles." Advances in Colloid and Interface Science 179–182: 123-132.

Wu, Z., H. Chen, Y. Dong, H. Mao, J. Sun, S. Chen, V. S. J. Craig and J. Hu (2008). "Cleaning using Nanobubble: Defouling by electrochemical generation of bubbles." Journal of Colloid and Interface Science 328(1): 10-14.

Xiong, Y. and F. Peng (2015). "Optimization of cavitation venturi tube design for pico and nano bubbles generation." International Journal of Mining Science and Technology 25(4): 523-529.

Yıldırım, A., O., Gül, S., Eren, O., Kusvuran, E. (2011). "A comparative study of ozonation, homogeneous catalytic ozonation, and photocatalytic ozonation for C.I Reactive Red 194 azo dye degradation." Clean – Soil Air Water 39(8): 799-805.

Zheng, C., Yu, L., Huang, L., Xiu, J., Huang, Z. (2012). "Investigation of a hydrocarbondegrading strain, Rhodococcus ruber Z25, for the potential of microbial enhanced oil recovery." Journal of Petroleum Science and Engineering 81: 49-56.

Zhou, Z., Chow, R., Cleyle, P., Xu, Z., Masliyah, J. (2010). "Effect of dynamic bubble nucleation on bitumen flotation." Canadian Metallurgical Quarterly 49(4): 363-372.

CHAPTER 3. GENERATION OF POSITIVELY CHARGED NANOBUBBLE

3.1. Introduction

Controlling zeta potential of NB (i.e. negative and positive) plays a major role in bubble-mineral contaminants interaction, bubble-oil aggregates meanwhile bubble coalescence significantly influences several treatment and separation processes, such as flotation, oil-sand separation, organic reduction, and membrane defouling (Calgaroto 2014). In most cases, the adsorption of the OH^- group (caused by the enthalpy difference in hydration between OH^- and H^+ ions) was dominant at the interface of the bubbles and determined the negative sign of the bubble zeta potential in deionized water (Najafi 2007, Elmahdy 2008). In addition, the bubble zeta potential has been used to calculate the pH of solutions (Najafi 2007, Wu 2012). Recent studies focused on modifying the charge of air bubbles, by varying the pH and ionic strength of aqueous solutions: acidic/basic solutions were buffered adding several types of chemicals at different concentrations (Cho 2005, Najafi 2007, Wu 2012). However, there has been little investigation on the stability of positive NB (Ushikubo 2010) and the adapting mechanisms related to positive NB' size growth in surfactant solutions (especially in those containing trivalent metal ions). Bubbles stability could be encouraged by the repulsion process,

which is caused by electrical charges at the air-water interface and affects bubble coalescence. Overall, the appearance of a surface charge, improving the stability of NB in the solution, was attributed to the relative arrangement of the water structure at the bubble interface (Ushikubo 2010). The mentioned studies agreed on a critical magnitude of zeta potential (30 mV), which can produce a great repulsion force, avoiding coalescence and contributing to the persistence of NB.

In order to identify possible mechanisms at the base of positive NB' size growth, and understand the dependence of this parameter on the properties of additives in the solution, it can be useful to study the temporal evolution of several parameters. In this chapter, the author investigates 1) the generation of positive NB in the presence of tri-valence metal ions (i.e. Fe^{3+} and Al^{3+}), 2) the possible mechanisms explaining the positive NB creation: adsorption of adsorbed species in the solution, and 3) the behavior of positive NB in the presence of Al^{3+} (the most common coagulant added into water treatment technologies) at different concentration.

3.2. Methodology

3.2.1. NB generation

The NB were prepared by injecting a supersaturated liquid-gas dispersion in a mixing chamber and then causing the breakup of MBs in splitter (Teflon

hose). This breakage was related to the surface tension of the aqueous system, known as “local stress” on the bubble interface. In bulk solutions, surfactants and frothers induce a surface tension gradient which increases the instability of the MB interface (Chu 2016).

As shown in Figure 3.1, the NB formation system consisted of a 10-L acrylic reactor, a motor (TM90-A0553, output 120 W, voltage AC 220 V, current 0.65 A, rotational speed 3000 rpm), a pump (Yongwon 980 kPa, external diameter = 12 mm, flow-rate = 15 L/min), a 5-L mixing chamber, and two Teflon hoses (10 m length, 3 mm and 10 mm diameter, respectively). A compressor was used to inject air at the Teflon hose at a pressure of 6 bars and at a flow rate of 50 mL/min; then, this air was mixed with additive-containing water. A milky aqueous suspension of MBs was produced in the mixing chamber and then broken up into NB within the narrow Teflon hose, before it returned to the reactor.

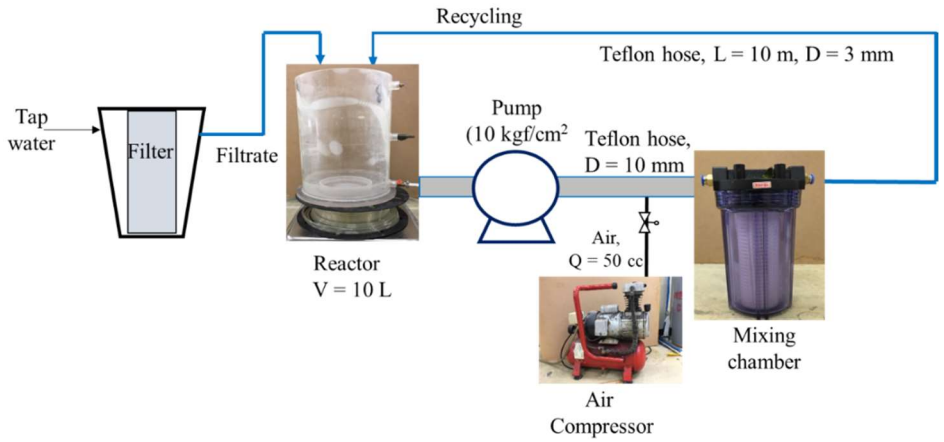

Figure 3.1. Schematic diagram of the experimental facility used to generate

NB: volume (V), diameter (D), flow rate (Q), and pressure (P).

The physical properties of the bubble were observed after the addition of different reagents such as dimethyldioctadecylammonium bromide (DODAB) ≥ 98%, Al^{3+} in $Al_2(SO_4)_3.18H_2O$ 98%, and Fe^{3+} in $FeCl_3 \cdot 6H_2O$ 98%. All chemicals were purchased from Daejung Chemicals & Metals Co., Ltd. (South Korea) and used after dilution in 5 L of filtered water in the acrylic reactor, as summarized in Table 3.1. Solution samples were collected from the reactor after 10 min of operation.

Table 3.1. Summary of used chemicals in the experiments (set 1: different reagents, concentration: 1 mM)

Chemicals	Structure	Ionic strength	Role in water treatment
DODAB	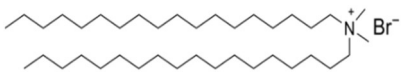	1.00×10^{-3}	Antimicrobial activity: Biological process and disinfection (Carmona-Ribeiro 2017)
$Al_2(SO_4)_3 – 18.H_2O$	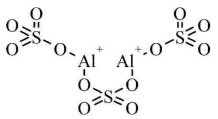	3.19×10^{-3}	Most widely-used coagulant: coagulation and flocculation process
$FeCl_3 – 6.H_2O$	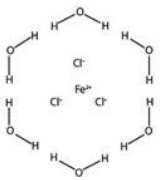	4.14×10^{-3}	Widely-used coagulant: coagulation and flocculation process

3.2.2. Experimental setup

Zeta potential of the NB along with average size were observed under different conditions: set 1 – addition of different chemical reagents: DODAB – a cationic surfactant, Al^{3+} and Fe^{3+} – the most common coagulants, chemical concentration: 1 mM, entire pH 2 ~ 12, observation time: 0 ~ 150 min; set 2 – addition of Al^{3+}: concentration from 0 ~ 10 mM, pH ~ 4, and observation time: 0 ~ 150 min.

3.2.3. NB size and zeta potential measurement

Dissolved oxygen (DO) concentration was measured using an optical DO meter (ProODO YSI Inc., USA), in order to confirm the quantity of supersaturated of gas in the NB generation system. In this study, the DO concentration was ~ 20.0 – 20.5 mg/L: much higher than the maximum DO saturation concentration at 25 °C (8.24 mg/L). All experiments were conducted in triplicate at room temperature. The bubble size and zeta potential were measured using a zeta potential-particle size analyzer (ELSZ-1000, Otsuka Electronics Co., Ltd., Japan). The instrument detects the particle with the size range of 0.6 ~ 10 000 nm, zeta potential value of -200 ~ +200 mV under concentration of 0.1 ~ 400 000 ppm. Due to electro-osmosis measurement and plot analysis, this instrument enables to provide high

precision analysis of zeta potential and size using micro-volume flow cell and disposal cell, respectively. This instrument measured the size of NB by dynamic light scattering (DLS). The size of NB, was obtained using polystyrene cuvettes (single use). It is confirmed that the DLS method can be used to observe nano-sized bubbles, which ranged between of ~ 30-250 nm (Kikuchi 2009) and > 290 nm (Najafi 2007).

In this study, measured concentration of NB at which the measurements were carried out was ~ $1.62 \times 10^6 \pm 1.2 \times 10^5$ particles per min. Due to advanced backscatter system, zeta potential – particle analyzer greatly offset multiple scattering influences from the calculation near the cell wall (Stetefeld 2016). In addition, backscatter system significantly boost the measured concentration for single scattering (Stetefeld 2016), so that it is not suffered from multiple scattering.

Before the zeta potential measurements, the samples were transferred into a flow cell (high concentration cell, made of glass with a path length of 1.5mm, between two platinum electrodes). The measured zeta potential was converted using Smoluchowski's equation, as follow:

$$\zeta = \frac{\mu K A \nu}{\varepsilon_r \varepsilon_0 \dot{i}} \qquad (3.1)$$

Where μ is the dynamic viscosity of the electrolyte solution (Pa·s), ε_r is the relative dielectric permittivity, ε_0 is the dielectric permittivity of vacuum, ν is the horizontal velocity of bubble (m/s), K is the measured electrolyte conductivity (S/m), and A is the cross-sectional area of the electrophoretic unit (m^2). Under measurement condition, values of the affecting factors were obtained as considering a viscosity of 8.83 x 10^{-4} Pa.s, a dielectric constant of 27.83, a refractive index of 1.3328, and a base frequency of 123.8 Hz. The signs of the zeta potentials were obtained from the pH (oscillating between 2 and 12) and measured within a timeframe of 150 min, at 30-min increments. Hereafter, we proposed the possible mechanisms of size growth and positive NB creation in such solutions. Due to Brownian motion and low rising velocity (Temesgen 2017) the NB convection and buoyancy can be considered negligible for these samples.

3.3. Positively charged NB generation in different reagent solutions

3.3.1. Creation and average size of NB

During the production of bubbles in the presence of chemical additives, > 83% of the bubbles were nano-sized (diameter ≤ 1 μm; (Temesgen 2017)). The initial bubbles produced in filtered tap water had instead an average diameter of 490 nm. Overall, the NB in the metal ion solutions were slightly

smaller than those in the cationic surfactant solutions, having average diameters of 450 – 600 nm and 500 – 680 nm, respectively. The results were obtained through DLS, which detects the Brownian motion of particles with diameters between 0.6 nm and 6 μm (Ushikubo 2010). Our results indicate a significantly high generation of NB in the presence of additives in the Teflon hose (using as a special splitter).

Table 3.2 shows that solution pH effects on NB size are relatively small. When looking at NB size variation with pH, (Cho 2005) reported that bubble size stayed similarly at ~ 750 nm in the entire pH 2 – 12. In addition, (Meegoda 2018) confirmed that the gas pressure and gas flow rate are major contributors to bubbles size. Hence, it is concluded NB size had no dependency on solution pH.

Table 3.2. Average size (nm) of NB in various solution pH

pH of solution		2	4	7	9	12
Average size of NB in the addition of	DODAB	552	524	513	542	552
	Al^{3+}	543	552	532	537	527
	Fe^{3+}	592	574	583	590	569

Figure 3.2 shows NB size for different types of solutions. As seen, bubbles in the DODAB and tri-valence metal ions became submicron-sized after 90 min.

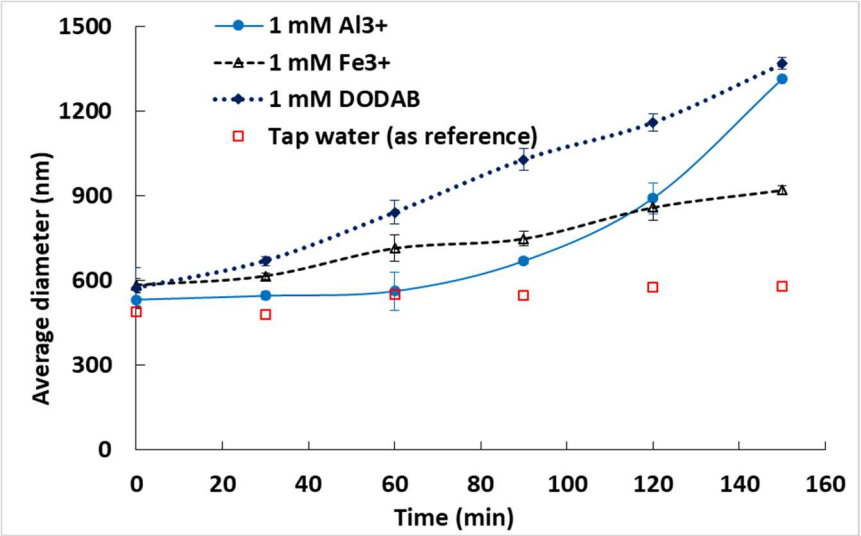

Figure 3.2. Temporal changes in the average NB diameter (size), in the presence of different chemical reagents. The data were obtained in triplicate and the error bars show the standard deviation.

An increase in size obtained in the presence of DODAB, Al^{3+}, and Fe^{3+} after 90 min confirms that several NB would coalesce (expressed by the number of coalesced bubbles), creating MBs in such solutions. Here, we suggest a simple equation to express the number of NB that came in contact with each other over time (the bubbles were assumed to be spherical):

$$n_2 \frac{4}{3}\pi(D/2)^3 = n_1 \frac{4}{3}\pi(d/2)^3 \qquad (1)$$

Where D is the size of coalesced NB at a specific time (nm), n_1/n_2 is the number of coalesced NB, and d is the initial size of coalesced NB (nm). The number of coalesced bubbles in the solutions, during the 150-min observation period, is indicated in Table 3.3.

It is still challenging to explain the bubble coalescence mechanism because of its rapid evolution. In an earlier report (Kracht 2009), bubble coalescence was estimated to occur within milliseconds. The basic process seems to involve the creation of a small region of organized water and with a single NB, through the diffusion and adsorption of surfactants; this region would then affect bubble contacts (Finch 2006). Similar mechanisms have been discussed concerning the presence of inorganic salts, like NaCl (Finch 2008, Kracht 2009): the total stress model of the solution (with viscoelastic properties and dilation viscosity) would be related to the mechanism of bubble coalescence. Here, the numbers referring to the quantity of coalesced bubbles are not integers: $n_1/n_2 = 3.9$ for Fe^{3+}, $n_1/n_2 = 13.6$ for DODAB, and $n_1/n_2 = 15.1$ for Al^{3+} at the end of the observation time (after 150 min; Table 3.3). The calculation relates the volume (V) and diameter (D and d) of the bubble, assuming that the number of coalesced bubbles is a function of the bubble

shape (S) and chemical properties (p) ($n = f(S, p)$). Moreover, it was assumed that the shape of bubbles was spherical, in order to obtain an ideal shape coefficient (S = 1); in fact, for S =1 the effect of bubble shape on the calculations is negligible. The properties of the reagents added to the solution (p) (e.g., ionic strength, surface tension, concentration, activity, etc.) may have additional effects on NB coalescence. More detailed investigations on the effects of p, could help to bring the application of the number of NB contacted (n) to predict other systems will be gained more attention in the further researches.

Table 3.3. Number of coalesced bubbles during the observation period (at pH 7).

Reagent solutions		Observation time (min)				
		30	60	90	120	150
Number of NB coalesced	DODAB	1.6	3.2	5.8	8.3	13.6
	Al^{3+}	1.1	1.2	2.0	4.7	15.1
	Fe^{3+}	1.2	1.8	2.1	3.2	3.9
	Water	1.0	1.1	1.5	1.7	1.7

3.3.2. Zeta potential of NB

Changes under variable pH

The solution had a neutral pH in the presence of DODAB (pH 6.83) but an acidic pH in the presence of Fe^{3+} (pH 2.35), and Al^{3+} (pH 4.11). When 1 mM DODAB was added in the solution, the NB were charged positively over a pH range of 2 – 12. Figure 3.3 shows a decrease in the positive zeta potential value with increasing pH (~ +40 ± 2 mV) for pH = 2, and ~ +20 ±5 mV for pH = 12). Similar trends have been reported in earlier studies. For example, the surface charge of NB dropped from ~ +50 mV to ~ +35 mV increasing the pH from 3 to 12 in a cetyltrimethylammonium bromide (CTAB) solution (Kim 2000), and from ~ +18 mV to ~ 0 mV increasing the pH from 3.5 to 10.5 in a dodecyltrimethyl ammonium chloride (DTAC) solution (Jia 2013). The DODAB, which is a double-chain cationic surfactant, could induce a bilayer adsorption of dioctadecyldimethylammonium ($DODA^+$ or $C_{30}H_{80}N^+$) at the air-water interface. In this case, the adsorption of $DODA^+$ was dominant, while the effect of H^+ on the zeta potential was negligible for pH > 7; resulting in a drop of zeta potential from +35 ± 2 mV to +20 ± 3 mV. At pH > 9, the zeta potential values remained stable (~ +20 ± 5 mV) for pH > 9. The positive charge resulted from the positivity of the adsorption layer that is greater than negativity of the bubble inner surface.

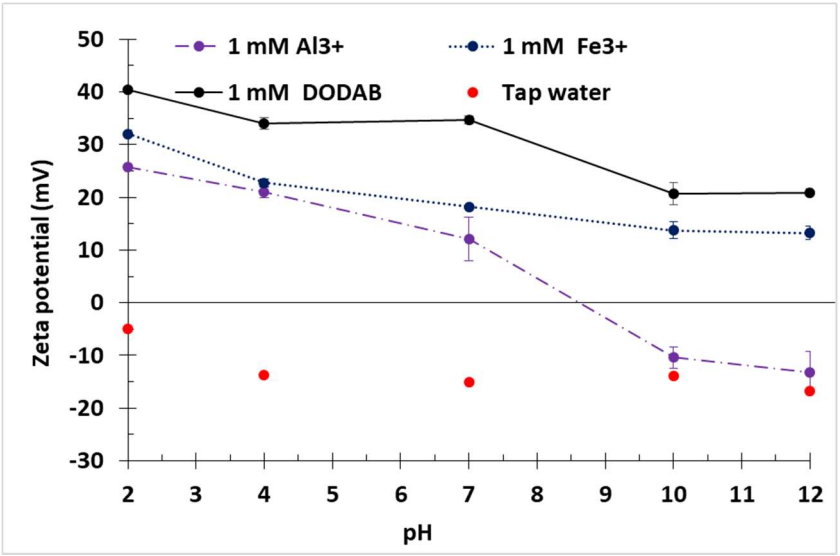

Figure 3.3. Zeta potential of bubbles as a function of pH, in the presence of different chemical reagents.

Overall, positively charged NB were obtained after the addition of trivalent metal ions (except for pH > 8.6 in case of Al^{3+}) at a concentration of 1 mM. The absolute value of their charges decreased with increasing pH. Specifically, in the presence of Al^{3+}, the charge of NB dropped from ~ +25 ± 1 mV to ~ -13.82 ± 1.55 mV while the pH increased from 2 to 12. In case of Fe^{3+} addition, positivity of the NB gradually decreased from ~ +32 ± 2.43 mV to ~ +13.25 ± 1.13 mV in the entire pH of 2 to 12.

Considering the case of Al^{3+} addition, figure 3.4 illustrates the species which can be formed in relation to pH: [Al^{3+}] were predominant at low pH, and their adsorption caused higher positive zeta potential values. As seen in Figure 3.4,

$Al(OH)_{3s}$ and $Fe(OH)_{3s}$ were formed in the pH of 4.1 ~ 10 and 2~ 12, respectively. In these entire pH, zeta potential values of the NB maintained positively; confirming the significant impacts of the hydroxide precipitates on the NB zeta potential. Indeed, in the absence of hydroxide precipitates the zeta potential of NB were lower than that with hydroxide precipitates and at several pH, the NB charged negatively (in the pH > 7.5 for the case of $Al(OH)_{3s}$); as provided in Figure 3.4. The presence of the metal ion species on its surface is similar to that on particle surface. Considering the case of the most common coagulant as Al^{3+}, the distribution of Al^{3+} species on negative particle surface is a function of pH. At acidic pH ranges (2 – 5) Al^{3+} is the major specie (obtained from the analysis in Visual minteq) and it can attach to the negative NB due to electrostatic attraction between them (Kim 2018). At pH 4 − 6, hydrolyzed aluminum species (i.e. $Al(OH)^{++}$, $Al(OH)_2^{+}$) are predominant, these species those have greater adsorption capacities due to strong chemical bonding and physical bonding between them (Hu 2017) would attach to negative NB. At pH 6 – 9, Al-hydroxide precipitate that is major specie bears positively charge and attaches on bubble surface (Lin 2012). These discussions therefore resulted in positive NB in the entire pH < 9. In contrast, at pH > 9 $Al(OH)_4^{-}$ cannot adsorb onto negative particle due to electrostatic repulsion mechanism (Kim 2018); thus, it is expected that zeta potential of NB

should be negative. These discussions indicate that the adsorption of the speciation of Al^{3+} in an aqueous solution can influence significantly NB zeta potential values.

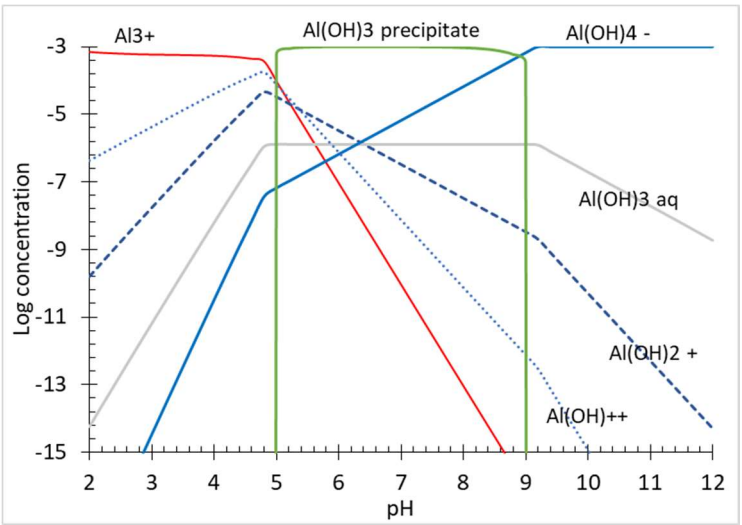

Figure 3.4. Aqueous speciation of 1 mM Al3+ at various pH levels. (Data obtained from Visual Minteq 3.1)

In most cases, the potentials reflect the adsorption of additives at the air-water interface when adding chemicals into NB generation system. In these solutions, mechanism of positive NB creation is exemplified in Figure 3.5 for the case of Al^{3+} addition; as it is a result of selective adsorption of specific Al^{3+} species at pH < 6 and/or due to precipitation of Al-hydroxide at pH 6 – 9 on the bubble interface.

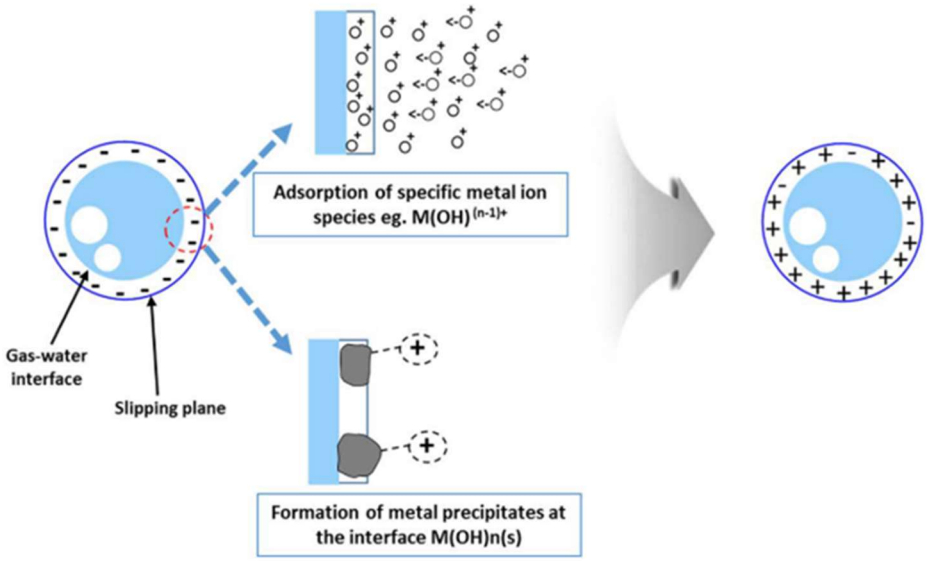

Figure 3.5. Proposed mechanism for the positive NB formation in the addition of Al^{3+}

Temporal changes

In order to observe the behavior of NB over time, all samples were maintained at a pH of 7. The zeta potential of initially formed NB (in filtered water) was negative (~ -15 ± 3 mV). Positive values were registered in the DODAB solution (Figure 3.7); the zeta potential of NB was ~ +40 ± 2 mV with a fluctuation around 0 mV for the whole 150-min period (Figure 3.7). These results prove the stability of bubbles in the bulk solution for at least the first 150 min. Prior works have documented bubble stability in several surfactant solutions via zeta potential analysis: there, the bubbles remained stable for a period of 60 min or up to > 24 hours (Saulnier 1996, Kim 2000,

Wu 2012). These studies agree with the results of our work: the ion adsorption carried out by additive head groups can not only influence the sign of the bubble surface charge, but also create a protective layer around the bubble and inhibit the dissolution of NB in surfactant solutions.

As seen in figure 3.6, positively charged bubbles were formed in trivalent metal ion solutions (i.e., Al^{3+} and Fe^{3+}). We observed changes in the charges of NB after the addition of a small amount of Al^{3+} ions. We also investigated the charges of NB in the presence of Fe^{3+} ions, another common trivalent metal ion: the positive charges were lower in the Fe^{3+} solution than in the Al^{3+} solution (~ +12 ± 0.5 mV at the initial measurement and ~ +15 ± 0.5 mV at the end of the 150-min observation period). Based on the zeta potential analysis, we confirmed that the presence of metal ions (Fe^{3+}, and Al^{3+}) improves NB stability in a solution: the zeta potential affected NB size, which is related to the accumulation rate of metal (positive) ions on the NB surface (Temesgen 2017).

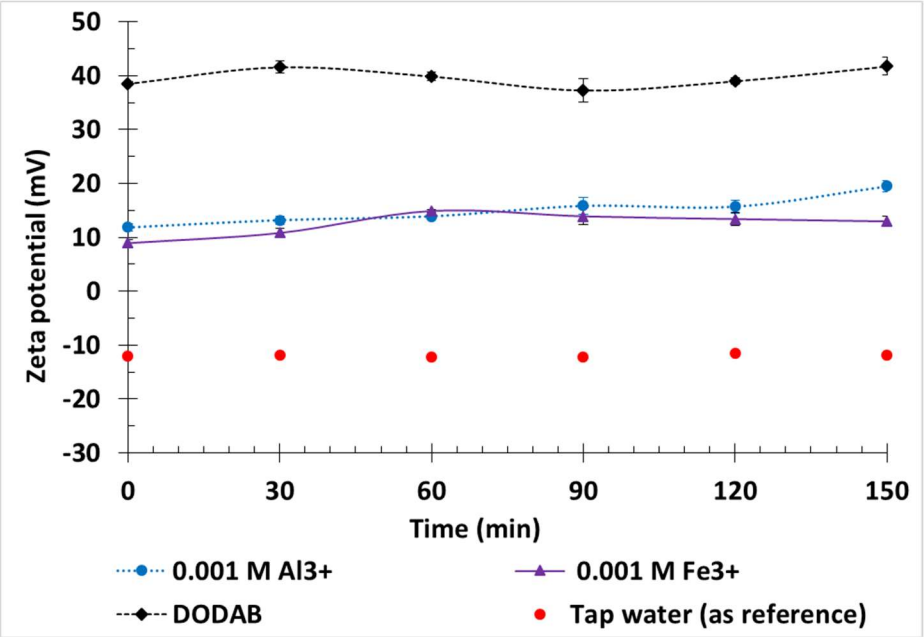

Figure 3.6. Evolution of bubble zeta potentials over time, in the presence of different chemical reagents at pH = 7. The graphs show the averaged values obtained from triplicate measurements; the error bars indicate the correspondent standard deviations.

3.4. Behavior of NB in the presence of various Al^{3+} concentration

Amongst the reagents that can result in the positive zeta potential for the NB, alum (Al^{3+}) is the most widely-used and economic coagulant in the water treatment and other particle separation process. Therefore, in this section, the author focused on the behavior of the positive NB under different concentrations of Al^{3+} (0 ~ 10 mM). Figure 3.7 indicates the average size and size distribution of bubbles for the addition of different Al^{3+} concentration. By

adding Al^{3+} into the bubbles generation system, ~ 90% of the bubbles was sized in nano-scale (diameter < 1 μm, according to the definition from (Temesgen 2017)). As seen in Figure 3.7, the average diameter of bubbles were in the range of 490 ~ 550 nm when adding 0 ~ 10 mM of Al^{3+}; showing that concentration of Al^{3+} had little effect on the NB size. Hence, our results confirm the high-precision NB generation in the absence and presence of Al^{3+} in the Teflon hose.

Figure 3.9 shows the sign and value of the NB zeta potential according to the concentration of Al^{3+} added. The NB are charged negatively in the absence of Al^{3+} and shifted positively in the presence of Al^{3+} > 0.5 mM. At 1 mM of Al^{3+} presence, the magnitude of the NB ZP was ~ +15 mV. Interestingly, at above 2 mM of Al^{3+} addition, the positive NB remained at ~ +20 mV, with fluctuation of 2 mV. In this study, 2 mM is the critical concentration of alum added for NB generation to obtain the stable positive value of the ZP. Negative and positive NB resulted from charge balance between negativity or positivity of adsorbed species and negativity of the inner surface at the interface of water-air. In the presence of 1 mM Al^{3+}, solution had pH of 4.11 (as discussed in section 3.3.2) and the pH slightly dropped to 3.833 when increasing Al^{3+} concentration up to 10 mM. In the experimental conditions, i.e., pH = 4 when adding 2 mM Al^{3+}, the solution has an ionic strength of 5.82×10^{-3}, sum of cations and anions of 4.12 meq/kg and 0.75 meq/kg, respectively, and the

charge difference of 69.3% (calculated from Visual Minteq 3.1). At pH ~ 4 hydroxide precipitates was not dominant as compared with Al^{3+}, $Al(OH)^{++}$, and $Al(OH)_2^{+}$ and the positivity of NB was due to the adsorption of these cationic species; that created a significant positive adsorption or ligand layer at the NB interface to sufficiently yield a positive ZP.

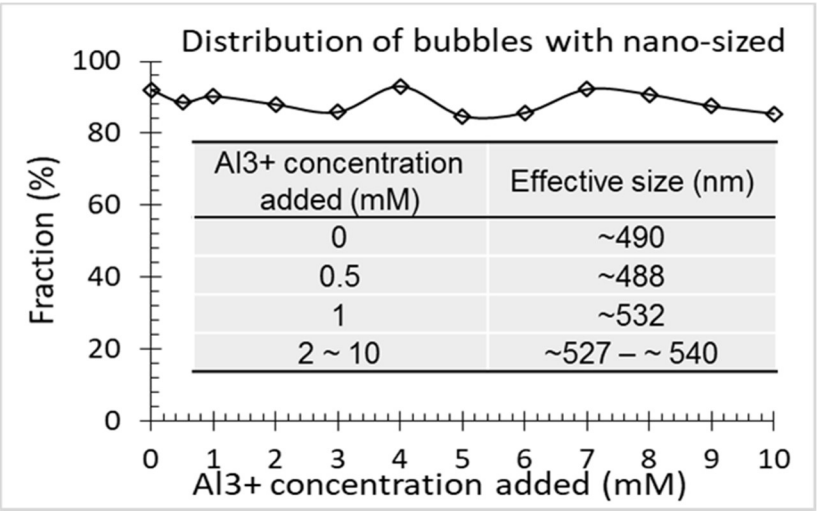

Figure 3.7. Average size of NB in various Al^{3+} concentration added

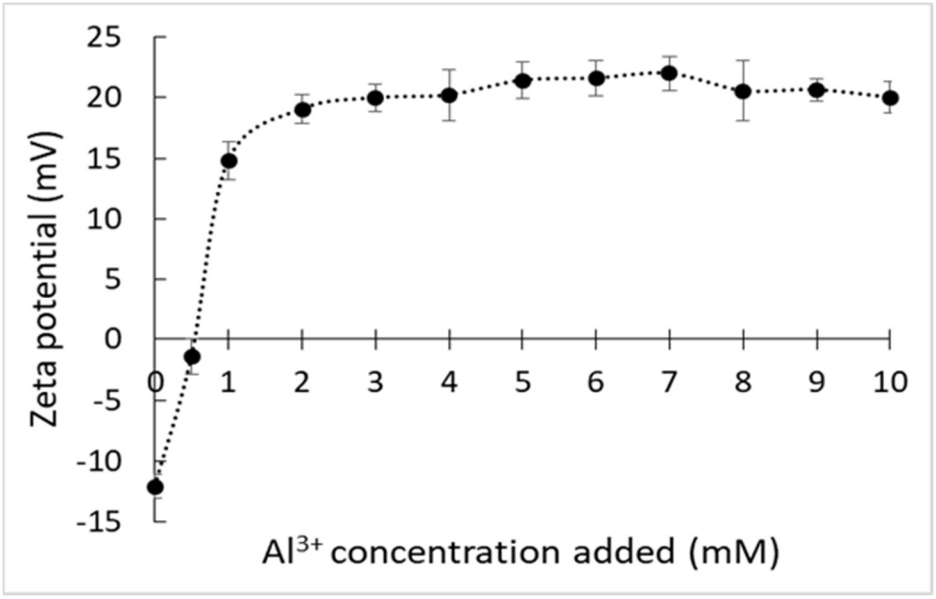

Figure 3.8. Zeta potential of NB in the presence of various concentration of Al^{3+}

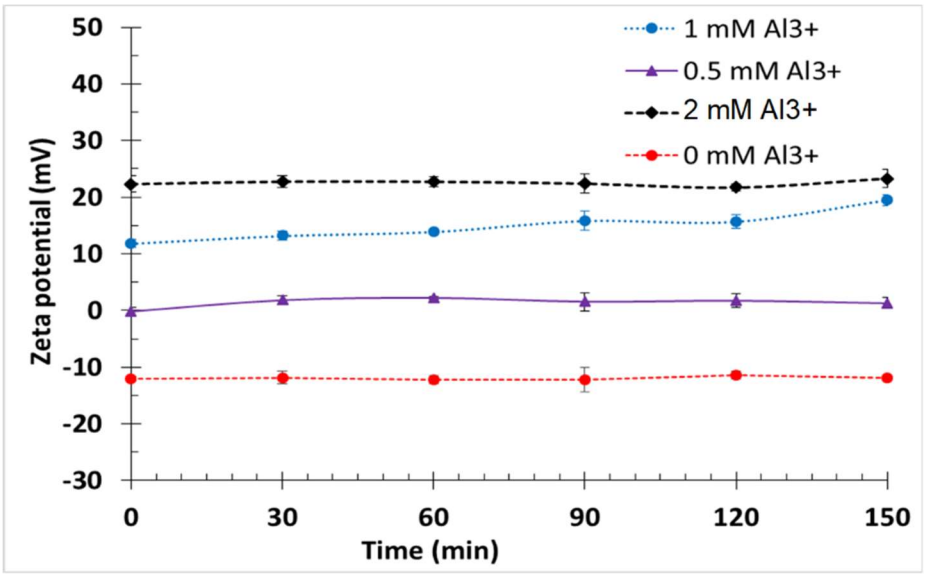

Figure 3.9. Temporal changes of NB zeta potential in the presence of Al^{3+}

Overall, the NB zeta potentials maintained at ~ -12 mV in the absence of Al^{3+} and ~ 0 mV for the case of 0.5 mM Al^{3+} with a fluctuation < 1 mV whereas the value of the positive zeta potential gradually increased with time, from ~ +12 ± 0.5 mV (initial measurement) to +20 ± 1 mV (at the end of the 150-min period); as provided in Figure 3.10. In this study, the remaining bubble surface charges in various concentration of Al^{3+} support that idea that zeta potential values < 30 mV could inhibit bubble coalescence after the addition of the low concentration of metal ions.

3.5. Summary

Creation of the NB in the presence of DODAB, Al^{3+}, and Fe^{3+} was confirmed by the average size of ~ 500 nm. The size of NB was independent during the entire pH of 2 to 12 and increased over time of 150 min (the increment of 30 min). Possible mechanism of the size growth was due to the coalescence of the NB in such solution. In all cases, positive NB were formed and its positivity decreased when solution pH increased. It was demonstrated that positive zeta potential sign of NB remained over time. Considering the addition of the most widely-used coagulant such as Al^{3+}, the generation of positive NB was due to the adsorption of specific Al^{3+} species in pH < 6 and the formation of Al-hydroxide in pH 6 – 9 on the bubble surface. It was resulted that the concentration of Al^{3+} insignificantly affected the NB size;

however, the ZP shifted from negatively charged to non-charged and positively charged in the presence of 0, 0.5, and ≥ 1 mM Al^{3+}, respectively. It was found that at ≥ 2 mM Al^{3+} the maximum ZP of the NB was obtained at ~ +20 mV. Regardless to [Al^{3+}] added, the insignificant temporal change in the zeta potential confirmed the stability of the NB in the Al^{3+} solution; allowing the application of such NB for many environmental processes, especially for the area of water treatment and soil remediation.

References

Agarwal, A., Wun, J., Ng., Liu, Y. (2011). "Principle and applications of microbubble and nanobubble technology for water treatment." Chemosphere 84(9): 1175-1180.

Alves, L., A., Silva,A., J., B., Giulietti, M. (2007). "Solubility of d-Glucose in Water and Ethanol/Water Mixtures." Journal of Chemical and Engineering Data 526: 2166-2170.

Arturo, B.-T., Roberto, P.-G., Diego, M.-C. (2015). "Zeta potential of air bubbles conditioned with typical froth flotation reagents." International Journal of Mineral Processing 140: 50-57.

Calgaroto, S., Wilberg, K., Q., Rubio, J. (2014). "On the Nanobubble interfacial properties and future applications in flotation." Minerals Engineering 60: 33-40.

Carmona-Ribeiro, A. M. (2017). The Versatile Dioctadecyl-dimethylammonium Bromide. Application and Characterization of Surfactants. R. Najjar, Intech: 157-181.

Castro, S., Miranda, C., Toledo, P., Laskowski, J. S. (2013). "Effect of frothers on bubble coalescence and foaming in electrolyte solutions and seawater." International Journal of Mineral Processing 124: 8-14.

Cho, S.-H., Kim, J.-Y., Chun, J.-H., Kim, J.-D. (2005). "Ultrasonic formation of Nanobubble and their zeta-potentials in aqueous electrolyte and surfactant solutions." Colloids and Surfaces A: Physicochemical and Engineering Aspects 269: 28-34.

Chu, P., Waters, K., E., Finch, J., A. (2016). "Break-up in formation of small bubbles: Break-up in a confined volume." Colloids and Surfaces A: Physicochemical and Engineering Aspects

503: 88-93.

Elmahdy, A., M., Mirnezami, M., Finch, J., A. (2008). "Zeta potential of air bubbles in presence of frothers." International Journal of Mineral Processing 89: 40-43.

Fan, M., Tao, D., Honake, R., Luo, Z. (2010). "Nanobubble generation and its application in froth flotation (part I): nanobubble generation and its effects on properties of microbubble and millimeter scale bubble solutions." Mining Science and Technology (China) 20(1): 1-19.

Finch, J., A., Gelinas, S., Moyo, P. (2006). "Frother-related research at McGill University." Minerals Engineering 19: 726-733.

Finch, J., A., Nesset, J., E., Acuna, C. (2008). "Role of frother on bubble production and behaviour in flotation." Minerals Engineering 21: 949-957.

Galvin, K., P., Engel, M., D., Nicol, S., K. (1994). "The potential for reagent recycle in the ion flotation of gold cyanide-a pilot scale field trial." International Journal of Mineral Processing 42: 75-98.

Haarhoff, J., Edzwald, J. K. (2001). "Modelling of floc-bubble aggregate rise rates in dissolved air flotation." Water Science and Technology 43(8): 175-184.

Jia, W., Ren, S. Hu, B. (2013). "Effect of Water Chemistry on Zeta Potential of Air Bubbles." International Journal of Electrochemical Science 8: 5828 - 5837.

Jose, E., B.-A., Sergio, A. B.-R., Raul, G.-G., Alejandro, E.-B., Jose, A. P.-M., Guillermo, G.-A., Jose, L., N.-B. (2011). "Effect of Electrolytes in Aqueous Solution on Bubble Size in Gas-Liquid Bubble Columns." Industrial and Engineering Chemistry Research 50: 12203-12207.

Kikuchi, K., Loka, A., Oku, T., Tanaka, Y., Saihara, Y., Ogumi, Z. (2009). "Concentration determination of oxygen Nanobubble in electrolyzed water." Journal of Colloid and Interface Science 329(2): 306-309.

Kim, J., S., Song, M., G., Kim, J., D. (2000). "Zeta Potential of Nanobubble Generated by Ultrasonication in Aqueous Alkyl Polyglycoside Solutions." Journal of Colloid and Interface Science 223(2): 285-291.

Kracht, W., Finch, J., A. (2009). "Using sound to study bubble coalescence."

Journal of Colloid and Interface Science 332: 237-245.

Li, C., Somasundaran, P. (1991). "Reversal of Bubble Charge in Multivalent Inorganic Salt Solutions - Effect of Magnesium." Journal of Colloid and Interface Science 146(1): 215-218.

Meegoda, J., N., Hewage, S., H., Batagoda, J., H. (2018). "Stability of Nanobubble." Environmental engineering science 35: 1216-1227.

Najafi, A., S., Drelich, J., Yeung, A., Xu, Z., Masliyah, J. (2007). "A novel method of measuring electrophoretic mobility of gas bubbles." Journal of Colloid and Interface Science 308: 344-350.

Quinn, J., J., Sovechles, J., M., Finch, J., A., Waters, K., E. (2014). "Critical coalescence concentration of inorganic salt solutions." Minerals Engineering 58: 1-6.

Saulnier, P., Lachaise, J., Morel, G., Graciaa, A. (1996). "Zeta Potential of Air Bubbles in Surfactant Solutions." Journal of Colloid and Interface Science 182: 395-399.

Sovechles, J., M., Lepage, M., R., Johnson, B., Waters, K., E. (2016). "Effect of gas rate and impeller speed on bubble size in frother-electrolyte solutions." Minerals Engineering 99: 133-141.

Stetefeld, J., McKenna, S., A., Patel, T., R. (2016). "Dynamic light scattering:

a practical guide and applications in biomedical sciences." Biophysical Reviews 8(4): 409–427.

Takahashi, M. (2005). "ζ Potential of Microbubbles in Aqueous Solutions: Electrical Properties of the Gas−Water Interface." The Journal of Physical Chemistry B 109(46): 21858-21864.

Temesgen, T., Bui, T. T., Han, M. Y., Kim, T.-I., Park, H. J. (2017). "Micro and nanobubble technologies as a new horizon for water-treatment techniques: A review." Advances in Colloid and Interface Science 246: 40-51.

Tsai, J., C., Kumar, M., Chen, S.-J., Lin, J.-G. (2007). "Nano-bubble flotation technology with coagulation process for the cost-effective treatment of chemical mechanical polishing wastewater." Separation and Purification Technology 58: 61-67.

Uchida, T., Liu, S., Enari, M., Oshita, S., Yamazaki, K., Gohara, K. (2016). "Effect of NaCl on the Lifetime of Micro- and Nanobubble." Nanomaterials 6(2): 31-40.

Ushikubo, F., Y., Furukawa, T., Nakagawa, R., Enari, M., Makino, Y., Kawagoe, Y., Shiina, T., Oshita, S. (2010). "Evidence of the existence and the stability of nano-bubbles in water." Colloids and Surfaces A: Physicochemical and Engineering Aspects 361: 31-37.

Usui, S. (1984). "Electrical Phenomena at Interfaces " Surfactant Sciences

Series 15: 30.

WHO (1998). Guidelines for drinking-water quality, 2nd ed. Health criteria and other supporting information. Geneva.

Wu, C., Nesset, K., Masliyah, J., Xu, Z. (2012). "Generation and characterization of submicron size bubbles." Advances in Colloid and Interface Science 179-182: 123-132.

CHAPTER 4. DECOLORIZATION OF RIT DYE USING POSITIVELY CHARGED NANOBUBBLE TECHNOLOGY

4.1. Objectives

The objective of this chapter were to prove the decolorization of a Rit dye in the presence of NB and observe the role of positive NB and reactive species on color removal efficiency. The assessment of Rit dye removal was performed by comparing the following processes: coagulation with Al^{3+} (2 mM), and oxidation with H_2O_2 (1 mM), NB alone, and NB/H_2O_2. Effects of the ideal ZP values (based on the amount of Al^{3+} added) and reactive species for the removal of Rit dye were observed in the presence of NB alone, ultrasonic NB, and NB/H_2O_2. The results from this study confirm that the NB processes are reliable evidence for the decolorization of polluted waters.

4.2. Experimental

4.2.1. In coagulation and oxidation processes

The dark green dye used in this study was Rit all-purpose powder dye; 31.9 g of it containing sodium chloride and anionic and non-ionic surfactants were used. In this study, Rit dye was dissolved in a 1-L acrylic reactor containing tap water at two concentrations, ~ 1200 and ~ 500 CU. Coagulant as aluminum

(Al^{3+} in $Al_2(SO_4)_3$, 98%) and oxidant as hydrogen peroxide (H_2O_2, 35%) were used as purchased from Sigma–Aldrich (South Korea).

Coagulation and oxidation processes were tested with a jar tester (Model: PHIPPS 7790 – 902, Phipps & Bird, USA). Water containing Rit dye was mixed for 1 min at 250 rpm, followed by the addition of reagents (i.e., Al^{3+} (2 mM) for coagulation and $H_{2]}O_2$ (1 mM) for oxidation) at 30 rpm; this slow regime was performed in 30 min. The samples were collected from the bottom of the reactor after 1 h of the treatment.

4.2.2. In NB technologies

In NB processes, the charged NB were created from a system as presented in chapter 3. To decolorize Rit dye in water, the charged NB were injected into a cylindrical reactor (made of acrylic, D x H = 100 mm x 450 mm, mixing speed of 150 rpm in 20 min) with a bubble rate of 30%. The NB-based processes, i.e., NB alone, ultrasonic NB, and NB/H_2O_2, were performed under operational conditions. NB: aluminum addition of 0 to 10 mM, ultrasonication: P = 400 W, and H_2O_2 1 mM. Furthermore, the color removal efficiency at an optimal concentration of alum addition was investigated within a timeframe of 150 min at 30-min increments. The schematics of color removal by the NB-based processes are shown in Figure 4.1.

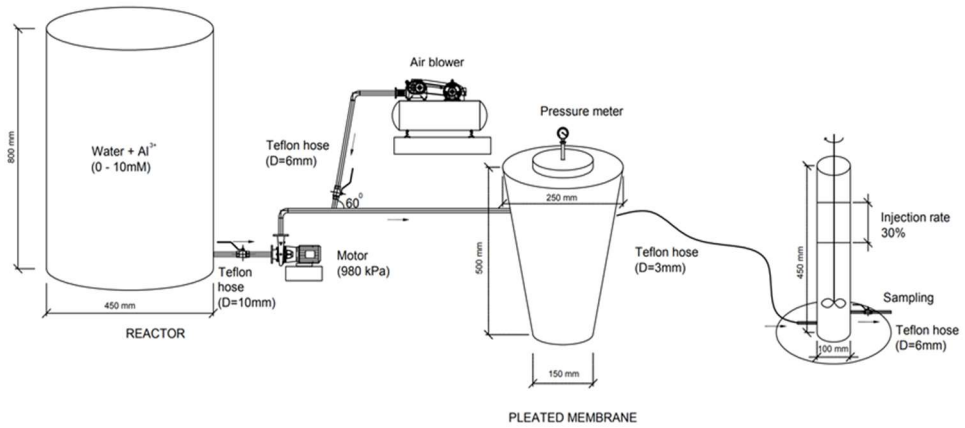

Figure 4.1. Schematics of decolorization of Rit dye by NB processes

4.3. Bubble properties observation and hydroxyl radical determination

Physical properties of bubbles, i.e. size and zeta potential, were obtained from a zeta potential-particle size analyzer (ELSZ1000, Japan). This instrument provides a high-precision analysis of bubble size and zeta potential in the range of 6 nm ~ 10 μm and of −200 ~ + 200 mV, respectively. The size of bubbles was obtained from dynamic light scattering method by transferring 2 mL (with a concentration of 5.5 x 10^6 ± 1.5 x 10^5 particles per minute) of samples into a single-use polystyrene cuvette. In zeta potential analysis bubbles were inserted into a flow cell between two platinum electrodes; the measurement was conducted under conditions: a viscosity of 8.83 x 10^{-4} Pa s, a relative dielectric permittivity of 27.28, dielectric permittivity of 1.783, and conversion of Smoluchowski's equation. Possible aqueous species of Al^{3+}-

solution (0~10 mM) were achieved from Visual Minteq 3.1 – a freeware chemical equilibrium model to observe the adsorption of Al^{3+} speciation for a positive NB creation.

Hydroxyl radical ($OH^{\cdot}$) in NB systems could be trapped in dimethyl sulfoxide (DMSO)(de Lunaa 2013, Fernández-Castro 2015) to produce methane sulfonic acid (MSA). In the present study, a solution of 700 μM DMSO (100 mL) was injected into 100 mL of NB solution for 12 min. Visible absorbance spectra for MSA products derived from the reaction of NB with DMSO were obtained by using UV spectrophotometer (HS-3300, HUMAS) at wavelength of 369 nm. Also, the spectra of 0, 10, 20 and 50 μM MSA (purchased from Sigma Aldrich) were observed to provide for reference.

4.4. Color measurement and quality control

For color measurement, standards having 20, 50, 100, 200, 500, and 1000 color units (CU) were prepared from the stock solution of 2000 CU that were made by dissolving 2.492 g potassium chloroplatinate (K_2PtCl_6, 99%) and 2.00 g cobaltous chloride ($CoCl_2.6H_2O$, 95%) in water with 100 mL HCl (35%) and diluting to 500 mL. All chemicals used for the preparation of standards were received from Daejung Chemicals & Metals (South Korea).

The samples were stored in 100-mL amber vials at 4 °C and subsequently warmed up to room temperature for measurement. The preferred sample pH

was adjusted to 4 using HCl/NaOH. A visible UV spectrophotometer (HS-3300, HUMAS) was used to record the UV-vis spectra. The color was measured within 24 h by monitoring the absorbance at a wavelength of 526 nm (dominant wavelength value for green, according to the standard method – ALPHA/AWWA/WEF, 2005). The spectrophotometer was preprogramed with calibrations of the platinum–cobalt standards and a provided color was analyzed in every five samples in duplicate to obtain the precision.

4.5. Results and discussion

4.5.1. Color removal efficiency

The decolorization of the dark green Rit dye in the presence of Al^{3+}, H_2O_2, and NB was visibly estimated first, as shown in Figure 4.3. In both weak and strong colors (~500 and ~1200 CU, respectively), the combination of charged NB and H_2O_2 indicated the highest rate of dye removal, followed by positive NB only. Specifically, the removals of dark green Rit dye at ~500 and ~1200 CU are illustrated in Figure 4. Overall, all the reagents were more efficient in decolorizing the lower dye concentration (i.e., 500 CU compared to 1200 CU), confirming that the dye concentration affected the efficacy of the treatment processes.

Interestingly, we achieved decolorization rates of ~40.53% for 500 CU and ~30% for 1200 CU with the addition of alum 2 mM, and is approximately

similar to those with the addition of negative NB (with a color removal of ~36±1.21 % for 500 CU and ~27±3.26% for 1200 CU). In this study, the formation of aluminum hydroxides from Al^{3+} addition that results in the trapping of the colloidal particles (Tchamango 2017) would create dye-coagulant flocs. In the negative NB process, the key treatment factor is expected for the radicals that were generated from the pyrolysis of water molecules during microbubble collapse (Temesgen 2017). The similar efficiency observed upon the addition of both reagents can be related to the similar effects of aluminum hydroxides formed by Al^{3+} and of radicals generated by negative NB.

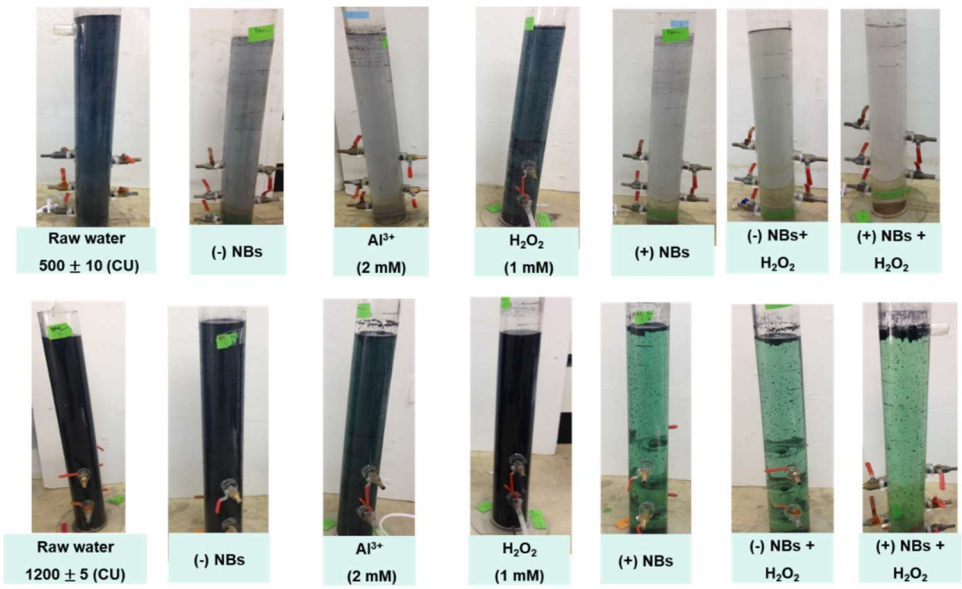

Figure 4.2. Visible decolorization of the dark green Rit dye in various reagents: $[Al^{3+}]$ = 2 mM, $[H_2O_2]$ = 1 mM, treatment time = 60 min.

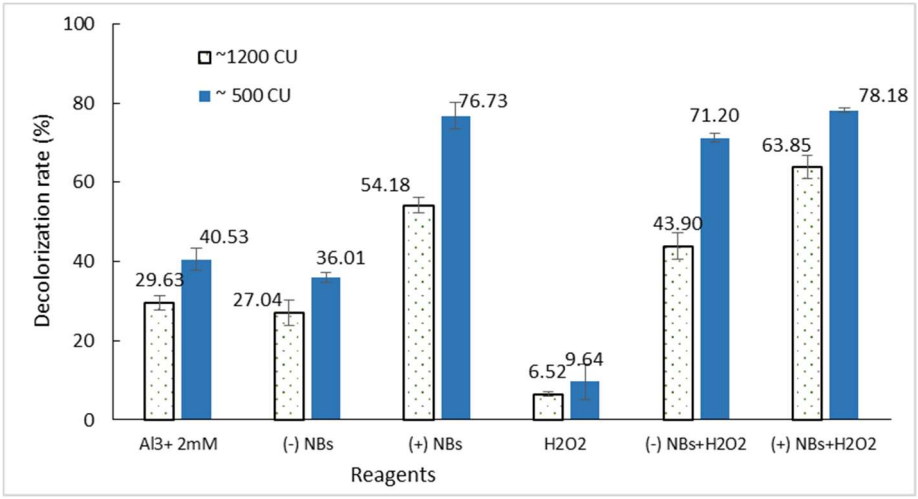

Figure 4.3. Decolorization of dark green dye in various reagents. Treatment time = 60 min, [H_2O_2] = 1 mM, [Al^{3+}] added into NB generation = 1 mM.

Hydrogen peroxide (1 mM) alone resulted in removal efficiencies of only 6.52±0.55 % for 1200 CU and 9.64±4.36 % for 500 CU after 60 min of oxidation. When we used the NB, the highest dye removal was obtained in the combination with H_2O_2 (~76±3.36 % for 500 CU and ~ 64±2.88 % for ~1200 CU), followed by the addition of positive NB alone, the combination of negative NB and H_2O_2, and negative NB alone. The results above suggest that NB significantly enhance the decolorization of Rit dye in the combination with H_2O_2 and that the treatment processes break the Rit dye molecules in the water. In many literature reviews, the decolorization of dyes has been studied comprehensively (Konsowa 2003, Tezcanli-Guyer 2003, Joo 2007, Jojeph 2009, Cai 2016, Quan 2017, Zhao 2018). As reported recently, H_2O_2 is

typically combined with UV (Basturk 2015, Moissa 2018), catalysts (Cardoso 2016, Moissa 2018, Paz 2018, Pang 2019), and cavitation microbubbles (Kumara 2009, Cai 2016) to achieve excellent decolorization performance. These researchers proposed various mechanisms that are related to the role of hydroxyl radicals and reactive species formed in the solutions on oxidizing the dyes, the degradation of dyes within bubbles, and supercritical reactions at the bubbles' interface. In this study, we found that the behavior of the Rit dye within negative NB is not dominant in decolorization, as demonstrated by the low color removal efficiency of ~27±3.26 %. Thus, the reactive species formed by the combination of NB and H_2O_2 and the supercritical reaction at the interface of the positive NB are likely to dominate Rit dye decolorization.

4.5.2. Optimization of charged NB processes

4.5.2.1. Effects of NB zeta potential and reactive species

Figure 4.4 summarizes the average size and zeta potential of the NB in various [Al^{3+}]. As discussed in Chapter 3, the NB had the size of ~ 500 to 530 nm and zeta potential of ~ -12, ~ 0, ~ +15, and ~ +20 mV in the addition of 0, 0.5, 1, and ≥ 2 mM Al^{3+}.

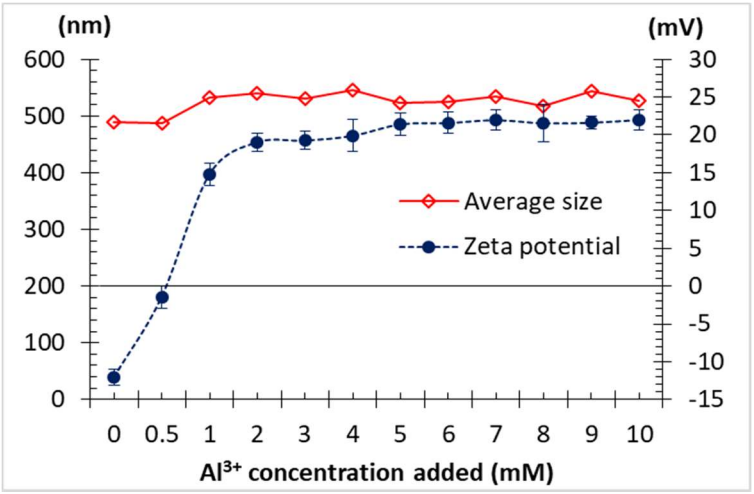

Figure 4.4. Average size and zeta potential of generation bubbles in different Al^{3+} concentration addition

Figure 4.5 indicates the decolorization rate of the Rit dye in the presence of NB alone, ultrasonic NB, and NB/H_2O_2 (1 mM). Considering an Rit dye concentration of ~1200 CU (Figure 4.5 – a), the color removal performances of the ultrasonic NB and NB/H_2O_2 processes were greater than that of the NB alone. Exceptionally, in the absence of Al^{3+}, the NB and NB/H_2O_2 could not efficiently degrade the Rit dye; the decolorization rates were only ~27±3.26 % and ~43±2.87 %, respectively. In contrast, the ultrasonic NB without the addition of Al^{3+} could remove up to ~67±1.45% of Rit dye after 1 h of the treatment. When we added Al^{3+} into the NB, the decolorization rate increased and the maximum removals of ~ 73±2.06 %, ~ 85±4.90 %, and ~ 90±4.08 %

were obtained in the presence of NB only, NB/H_2O_2, and ultrasonic NB, respectively.

We now consider the decolorization performance of these processes for an Rit dye concentration of ~500 CU. As shown in Figure 4.5 – b, an insignificant difference in color degradation degree occurred under the two conditions of NB, i.e. under ultrasonication and combined with H_2O_2. In general, the maximum color removal was obtained at ZP of NB ~ 20 mV (above 2 mM of Al^{3+} addition), at ~75±2.11 %, ~96±1.05 %, and ~98±0.54 % in the presence of NB only, ultrasonic NB, and NB/H_2O_2, respectively.

We found that the decolorization ratio of the Rit dye, especially at the concentration of ~500 CU, depended on the applied ZP values of the NB. Effects of ZP value on color degradation is typically observed in the process of NB alone. As reported by (Kumara 2009, Cai 2016), the reaction that occurred in the bubble interface may result in the dominant color removal; thus, in this case, the possible mechanism can be primarily related to the electrostatic attraction between the NB and dye components during the treatment process. In the present work, the surface charge of the Rit dye (containing non-ionic and ionic surfactant) was negative with a value of ~-17.05 mV (measured by zeta potential – particle size analyzer). Furthermore, negative NB showed its ineffectiveness in decolorizing the Rit dye, with a rate

of decolorization of ~ 36.01±4.05 % for ~ 500 CU of Rit dye. In contrast, the greater performance was obtained in the application of positive NB with zeta potentials from ~ +15 to ~ +20mV, as seen in Figure 4.5. The results confirm that color removal efficiency was optimized when (1) the charge of NB and dye solution were opposite and (2) the magnitude of NB surface charge was almost similar to the magnitude of the dye's surface charge in the solution.

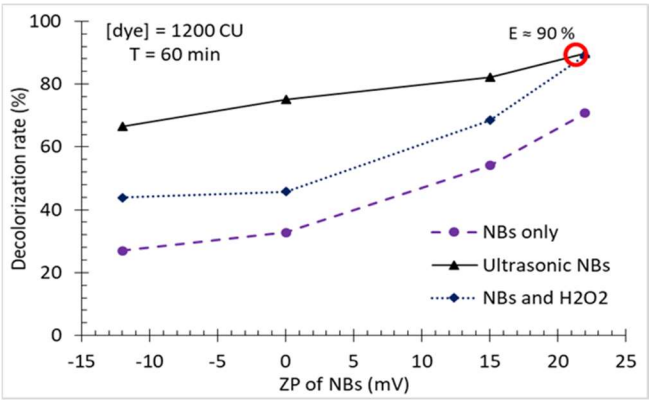

a

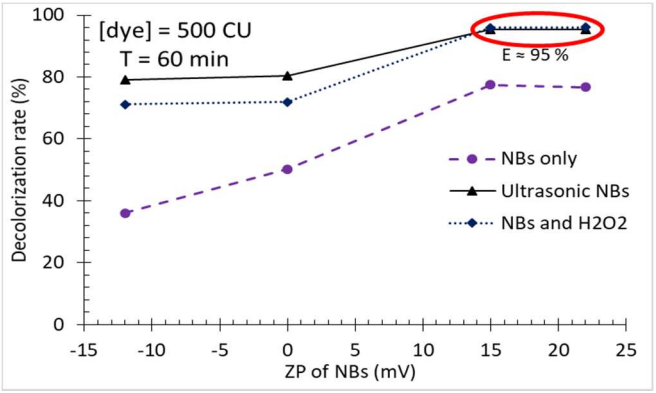

b

Figure 4.5. Decolorization of Rit dye by the NB processes. Treatment time = 60 min, ultrasonic power = 400 W, $[H_2O_2]$ = 1 mM.

An increase in color removal by ultrasonic NB and NB/H_2O_2 processes is also expected due to the role of free radicals in destroying Rit dye molecules. It is reported that the pyrolysis of water molecules during microbubble collapse generates reactive species such as $OH^{\cdot}$ radicals (Takahashi 2007, Temesgen 2017). To verify this deduction we examined $OH^{\cdot}$ generation in three NB systems (i.e. NB alone, ultrasonic NB, and NB/H_2O_2) by observing visible absorbance spectra of methane sulfonic acid (MSA) essay derived from the reaction of $OH^{\cdot}$ and a trapping reagent such as DMSO (Fernández-Castro 2015):

$$CH_3SOCH_3 + OH^{\cdot} \rightarrow CH_3SOOH + CH_3^{\cdot} \qquad (1)$$

Visible absorbance spectra for the production when adding DMSO into NB systems are provided in Figure 4.6. Three curves of the visible absorbance spectra of the MSA essay were similar in shape to the spectra of 0 mM and 50 mM MSA standards, being in excellent agreements with the inference that MSA was certainly formed to confirm the presence of $OH^{\cdot}$ in applied NB systems.

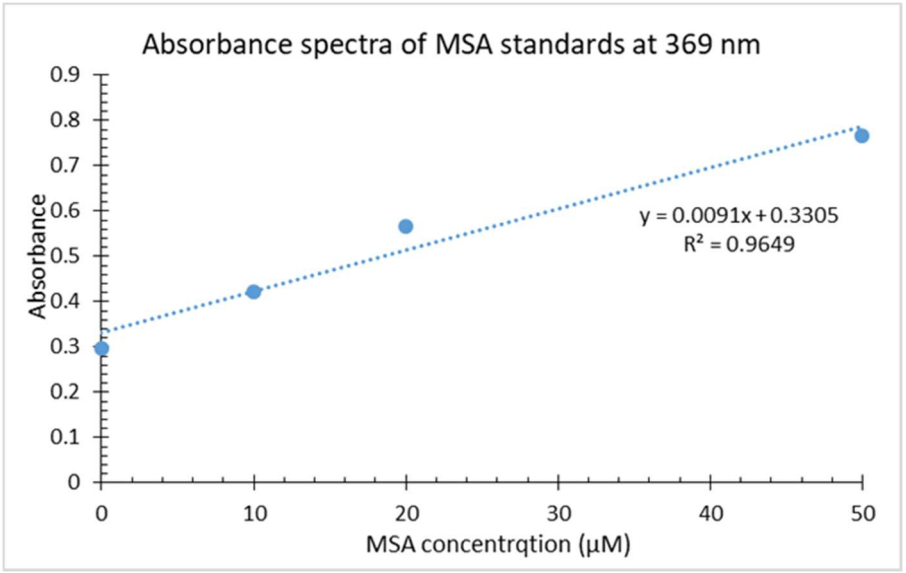

Figure 4.6. Visible absorbance spectra of MSA standards at the wavelength of 369 nm

Table 4.1. Quantification of MSA produced in the NB systems

Source	Absorbance	MSA (µM)
NB and DMSO (1)	0.41	8.41
Ultrasonic NB and DMSO (2)	0.60	29.18
NB/H2O2 and DMSO (3)	0.53	21.37
DMSO (4)	0.29	-
NB alone (5)	-	-
Ultrasonic NB (6)	-	-
NB/H2O2 (7)	0.27	-

It is obvious that as ultrasonic NB were applied, the Rit dye removal accelerated significantly (Figure 4.5). Perhaps the more amounts of $OH^{\cdot}$ affected the decolorization performance. As shown in Figure 4.6 and equation (1), the greatest concentration of MSA produced from DMSO in ultrasonic NB system (29.19 µM) demonstrated the enhancement of $OH^{\cdot}$ radical

generation and improved the oxidization of ultrasonic NB. Similar decolorization performance in NB/H_2O_2 system indicates that H_2O_2 is fundamental in enhancing the degradation of Rit dye and that the treatment process destroys the Rit dye molecules. In the presence of H_2O_2 and NB, other reactive species were produced through reactions with the $OH^{\cdot}$ radical, as follows (Toor 2006, Huang 2008, Ghodbane 2010):

$$OH^{\cdot} + H_2O_2 = H_2O + HO_2^{\cdot} \quad (2)$$

$$HO_2^{\cdot} + H_2O_2 = OH^{\cdot} + H_2O + O_2^{\cdot} \quad (3)$$

$$HO_2^{\cdot} + OH^{\cdot} = H_2O + O_2^{\cdot} \quad (4)$$

The formation of $HO_2^{\cdot}$ and $O_2^{\cdot}$ in reactions (2) to (4), owing to their strong oxidant properties to attack and destroy the dye molecules (Konsowa 2009, Paz 2018, Pang 2019) is expected to obtain the great decolorization rate of the Rit dye in the NB/H_2O_2 system. Furthermore, we found that $OH^{\cdot}$, $HO_2^{\cdot}$, and $O_2^{\cdot}$ in the NB/H_2O_2 system and $OH^{\cdot}$ in the ultrasonic NB system contributed similarly to the degradation of the Rit dye. The results, about > 85% of Rit dye decolorization, can be the reliable evidence to demonstrate the reactive species effect on the performance of ultrasonic NB and NB/H_2O_2 processes.

4.5.2.2. Decolorization rate vs. treatment time

Figure 4.7 illustrates the Rit dye (~1200 CU) removal based on the treatment time by the NB processes with ZP ~+15 mV and ~+20 mV. In

general, the treatment time insignificantly affected the decolorization rate in the presence of the ultrasonic NB. Specifically, decolorization by ultrasonic NB could achieve and maintain an excellent removal efficiency from the first 30 min, with a degradation degree of ~78% (Figure 4.7 – a). In contrast, Rit dye removal in the presence of NB alone and that of NB coupled with H_2O_2 was improved when the treatment time was increased. The experimental results indicated that less than 40% of the Rit dye was removed in these systems at 30 min and the degradation rates were increased up to ~78% in the NB system and ~83% in the NB coupled with H_2O_2 system at 150 min. Similar color removal trends were obtained in the presence of NB with ZP of +20 mV, except for the ultrasonic NB process (Figure 4.7 – b). As shown, the efficiency of Rit dye degradation by the ultrasonic NB process improved after 1 h of treatment and yielded the maximum efficiency of ~90%. Furthermore, the decolorization performances in the presence of NB (+20 mV) and NB (+20 mV)/H_2O_2 were greater in the first 30 min. These results evidence that NB with a higher positivity would enhance the degradation of Rit dye molecules within a shorter treatment time.

For weaker colors (i.e., ~500 CU), it appears that in each process, the ZP values of the NB insignificantly affected the color degradation, as shown in Figure 8. The presence of ultrasonic NB yielded a stable decolorization rate at ~90% during treatment time. In the first 60 min of treatment, the Rit dye

removals increased and subsequently remained at ~80% and ~95% in the presence of NB alone and NB coupled with H_2O_2, respectively. We suggest that an optimal decolorization time of 30 min for the ultrasonic NB, and 60 min in the presence of NB alone and NB combined with H_2O_2.

In ultrasonic NB system, the rising velocity of ultrasonic NB is expected to affect the decolorization time significantly. The increase in rising velocity, as a result from applying ultrasonic energy into the NB system, could accelerate the reaction kinetics of the $OH^{\cdot}$ radical and Rit dye molecules through the coalescence and collapse mechanisms of the NB in the solution. In the beginning, microbubbles were formed rapidly during the coalescence of the NB but soon collapsed to NB again and simultaneously increased $OH^{\cdot}$ radical generation (Temesgen 2017). Consequently, the driving force for the transfer of $OH^{\cdot}$ radicals and positive NB to the dye solution and the degradation of the Rit dye were completed, with a consequent decrease in decolorization time.

Figure 4.3 shows that a layer of bubble-Rit dye at the surface of the solution after 60 min of treatment in the presence of the positive NB and the charged NB/H_2O_2, confirming a transfer from the bubbly regime to the aggregate regime where the NB started to coalesce into larger bubbles. According to (Eskandarloo 2017), in the addition of anionic surfactants the

bubbles slowly increased their size because the surfactant descended the NB surface tension; and in our study, anionic surfactants in Rit dye impacted on the coalescence of the NB, resulting in a foam layer after 60 min of treatment. Moreover, as the contact between floating bubbles and the contaminants occurred when particles trapped in the foam layer (Kang 2019), the dye-NB regime requires a certain decolorization time.

The increase in decolorization time in the presence of NB and NB/H_2O_2 may be also attributed to the reaction kinetics of the reactive species and Rit dye molecules vs. the contact time. Particularly, the presence of NB alone and NB/H_2O_2 could efficiently decolor the Rit dye of ~500 CU within the first 60 min, as evidenced by the reactions at the NB interface that reached the equilibrium state. The data from Figure 4.7 and Figure 4.8 indicate that kinetics of Rit dye decolorization by NB and NB/H_2O_2 processes were first-order since the use of the second-order were not feasible with $R^2 < 0.95$. Rate constants (k_{obs}) were obtained for Rit dye removal in the presence of NB alone and NB/H_2O_2, as summarized in Table 4.2.

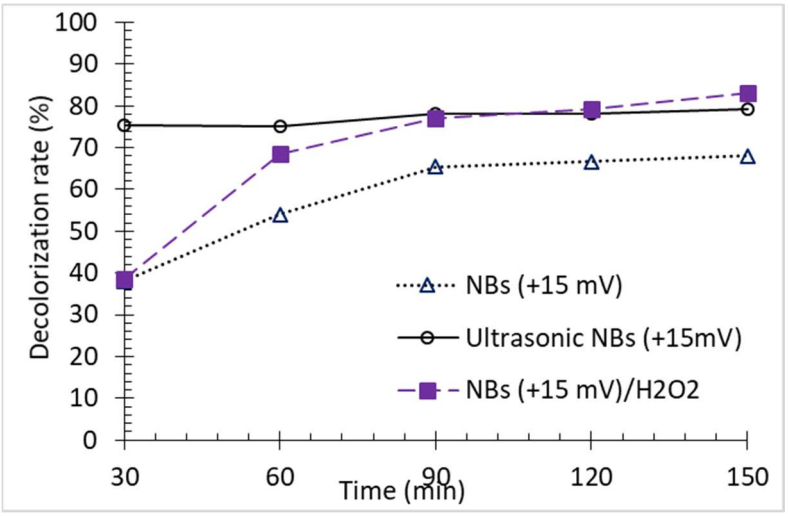

a

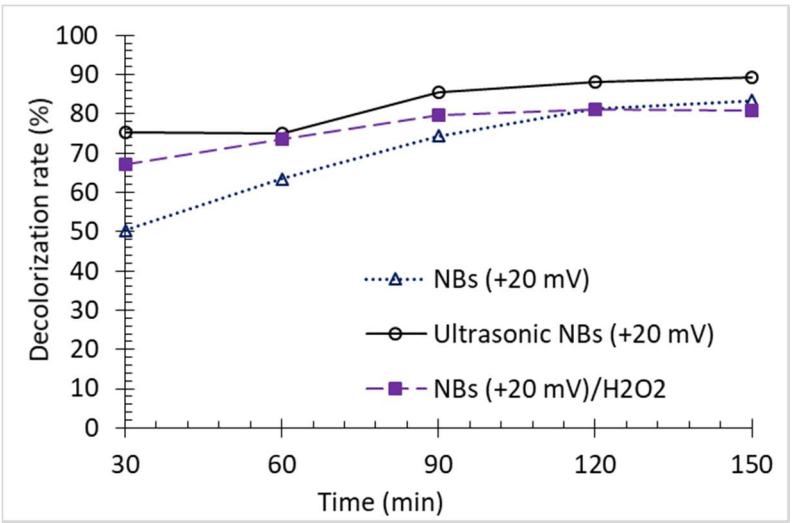

b

Figure 4.7. Rit dye removal over treatment time by processes of NB with ZP of +15 mV (left panel) and +20 mV (right panel). [Rit dye] = 1200 CU, pH = 3.0, ultrasonic power = 400 W, [H_2O_2] = 1 mM.

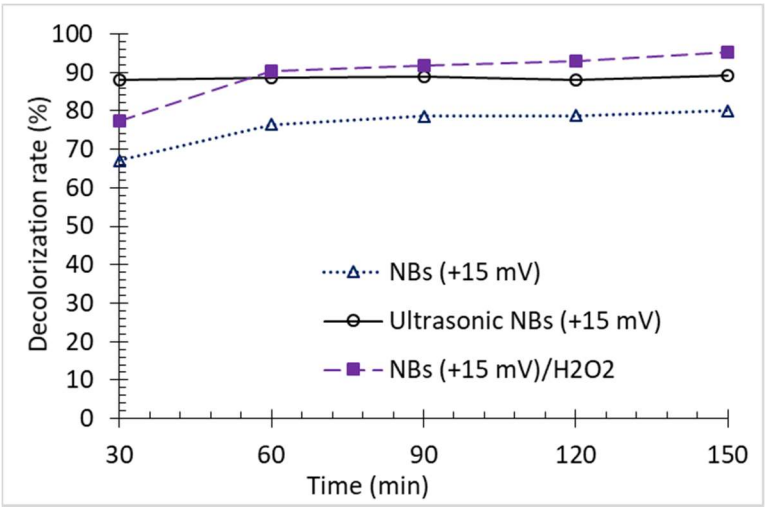

a

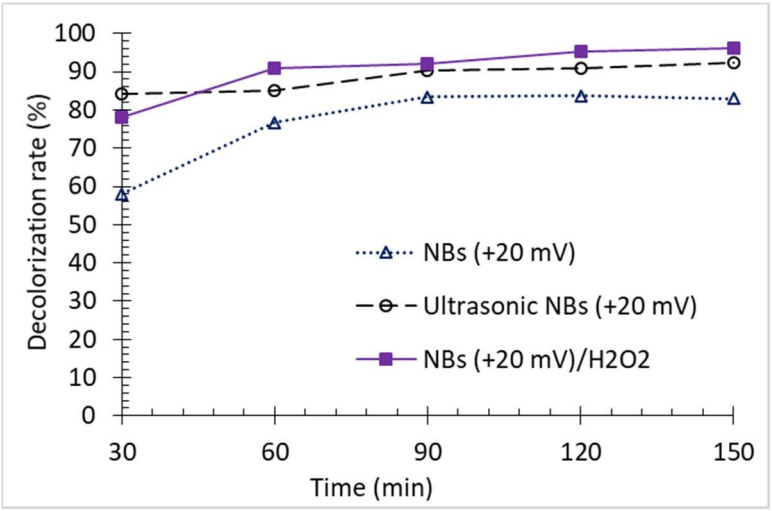

b

Figure 4.8. Rit dye removal over treatment time by processes of NB with ZP of +15 mV (left panel) and +20 mV (right panel). [Rit dye] = 500 CU, pH = 3.0, ultrasonic power = 400 W, [H_2O_2] = 1 mM.

Table 4.2. Rate constants for Rit dye decolorization by NB and NB/H_2O_2 processes

Rit dye concentration	k_{obs} (min^{-1})*			
	ZP = +15 mV		ZP = +20 mV	
	NB alone	NB/H_2O_2	NB alone	NB/H_2O_2
~1200 CU	~0.0033 (150 min)	~0.0108 (90 min)	~0.0045 (150 min)	~0.0146 (60 min)
~500 CU	~0.0055 (90 min)	~0.0132 (60 min)	~0.0092 (90 min)	~0.0154 (60 min)

* Calculated using equation $\ln C_t = \ln C_o - kt$

Rate constants of the reactions decreased when decolorization time increased. For example k_{obs} value of NB process was ~0.0033 with an efficiency of ~68% in 150 min; meanwhile, k_{obs} value of the process using NB/H_2O_2 was ~0.0146, leading the treatment time of 60 min with a decolorization rate of ~90%. The observation of rate constant shows that the processes carried out using NB/H_2O_2 overall provided the greater results in treatment time and color removal efficiency. However, the application of NB system in the decay of the Rit dye was also feasible, although it required longer treatment time.

4.6. Summary

The NB technologies are efficient for decolorization of Rit dye. The experimental results showed the fundamental role of the NB zeta potential and reactive species (i.e. $OH^{\cdot}$, $HO_2^{\cdot}$, and $O_2^{\cdot}$) for Rit dye decolorization significantly by the NB-based processes. Increase in the color concentration required longer treatment time and greater zeta potential of NB applied. In the present chapter, reaction mechanisms follow two possible paths such as electrostatic attraction and the oxidation drove decolorization of Rit dye in the NB systems. The rising velocity of the bubbles, the transfer from the bubbly regime to aggregate regime, and the reaction kinetics of the reactive species and Rit dye molecules was expected to lead the treatment time. Overall, the NB technique, especially the ultrasonic NB and NB/H_2O_2 processes, efficiently separate the color from polluted water because of the surface charge attraction between bubbles and dyes and the excellent oxidation by the reactive species.

References

Basturk, E., Karatas, M. (2015). "Decolorization of antraquinone dye Reactive Blue 181 solution by UV/H2O2 process." Journal of Photochemistry and Photobiology A: Chemistry 299: 67-72.

Cai, M., Su, J., Zhua, Y., Wei, X., Jin, M., Zhang, H., Dong, C., Wei., Z. (2016). "Decolorization of azo dyes Orange G using hydrodynamic cavitation coupled with heterogeneous Fenton process." Ultrasonics Sonochemistry 28: 302-310.

Cardoso, C., Bessegato, G., Zanoni, M. (2016). "Efficiency comparison of ozonation, photolysis, photocatalysis and photoelectrocatalysis methods in real textile wastewater." Water Reasearch 98: 39-46.

de Lunaa, M., D., G., Coladesa, J., I., Sub, C., C., Lu, M., C. (2013). "Comparison of dimethyl sulfoxide degradation by different Fentonprocesses." Chemical Engineering Journal 232: 418-424.

Eskandarloo, H., Kierulf, A., Abbaspourrad, A. (2017). "Nano- and micromotors for cleaning polluted waters: focused review on pollutant removal mechanisms." Nanoscale 9: 13850-13863.

Fernández-Castro, P., Vallejo, M., Román, M., F., S., Ortiz, I. (2015). "Insight on the fundamentals of advanced oxidation processes. Role and review of the

determination methods of reactive oxygen species." Journal of Chemical Technology & Biotechnology 90: 796-820.

Ghodbane, H., Hamdaoui, O. (2010). "Decolorization of antraquinonic dye, C.I. Acid Blue 25 in aqueous solution by direct UV irradiation UV/Fe(II) processes." Chemical Engineering Journal 160: 226-231.

Huang, M., Xu, C., Wu, Z., Huang, Y., Lin, J., Wu, J. (2008). "Photocatalytic discolorization of methyl orange solution by Pt modified TiO2 loaded on natural zeolite." Dyes and Pigments 77: 327-334.

Jojeph, C., G., Puma, G., L., Bono, A., Krishnaiah, D. (2009). "Sonophotocatalysis in advanced oxidation process: a short review." Ultrasonics Sonochemistry 16: 583-589.

Joo, D., J., Shin, W., S., Choi, J., H., Choi, S., J., Kim, M., C., Han, M., H., Ha, T., W., Kim, Y., H. (2007). "Decolorization of reactive dyes using inorganic coagulants and synthetic polymer." Dyes and Pigments 73: 59-64.

Kang, Y., G., Yoon, H., W., Lee, C., S., Kim, E., J., Chang, Y., S. (2019). "Advanced oxidation and adsorption bubble separation of dye using MnO2-coated Fe3O4 nanocomposite." Water Reasearch 151: 413-422.

Konsowa, A., H. (2003). "Decolorization of wastewater containing direct dye by ozonation in a batch bubble column reactor." Desalination 158: 233-240.

Konsowa, A., H. (2009). "Decolorization of wastewater containing direct dye by ozonation in a batch bubble column reactor." Desalination 158: 233-240.

Kumara, M., S., Sonawanea, S., H., Pandit, A., B. (2009). "Degradation of methylene blue dye in aqueous solution using hydrodynamic cavitation based hybrid advanced oxidation processes." Chemical Engineering & Processing: Process Intensification 122: 288-295.

Moissa, F., L., Mittersteiner, M., Saugo, R., Floriani, T., C., de Jesus, P., C. (2018). "Kinetic behavior of C.I. Reactive Blue 182 towards oxidation with H2O2/UV and H2O2/NaOH systems." Journal of Molecular Liquids 264: 675-682.

Pang, J., Fu, F., Li, W., Zhu, L., Tang, B. (2019). "Fe-Mn binary oxide decorated diatomite for rapid decolorization of methylene blue with H2O2." Applied Surface Science 478: 54-61.

Paz, E., C., Aveiro, L., R., Pinheuro, V., S., Souza, F., M., Silva, F., L., Hammer, P., Lanza, P., R., V., Santos, M., C. (2018). "Evaluation of H2O2 electrogeneration and decolorization of Orange II azo dye using tungsten oxide nanoparticle-modified carbon." Applied Catalysis B: Environmental 232: 436-445.

Quan, X., Luo, D., Wu, J., Li, R., Cheng, W., Ge, S. (2017). "Ozonation of acid red 18 wastewater using O3/Ca(OH)2 system in a micro bubble gas-liquid

reactor." Journal of Environmental Chemical Engineering 5(1): 283-291.

Takahashi, M., Chiba, K., Li, P. (2007). "Free-Radical Generation from Collapsing Microbubbles in the Absence of a Dynamic Stimulus." The Journal of Physical Chemistry B 111(6): 1343–1347.

Tchamango, S., R., Kamdoum, O., Donfack, D., Babale, D. (2017). "Comparison of Electrocoagulation and Chemical Coagulation Processes in the Treatment of an Effluent of a Textile Factory." Journal of Applied Sciences and Environmental Management 21(7): 1317-1322.

Temesgen, T., Bui, T. T., Han, M. Y., Kim, T.-I., Park, H. J. (2017). "Micro and nanobubble technologies as a new horizon for water-treatment techniques: A review." Advances in Colloid and Interface Science 246: 40-51.

Tezcanli-Guyer, G., Ince, N., H., Alaton, I., A. (2003). "Sonochemical destruction of textile dyestuff in wasted dyebaths." Coloration Technology 119: 292-296.

Toor, A., P., Verma, A., Jotshi, C., K., Bajpai, P., K., Singh, V. (2006). "Photocatalytic degradation of Direct Yellow 12 dye using UV/TiO2 in a shallow pond slurry reactor." Dyes and Pigments 68: 53-60.

CHAPTER 5. SEPARATION OF OIL-SAND USING POSITIVELY CHARGED NANOBUBBLE TECHNOLOGY

5.1. Objectives

The objectives of this chapter were to prove the oil-sand separation in the injection of the charged NB with respect to the effects of the NB/oil-sand ratio, the treatment time, and the NB injection regimes. The assessment of the oil-sand separation efficiency was presented by TPH removal. The results from this study confirm the major role of the positive bubbles coalescence on the flotation of the bubble-oil attachment under experimental operations.

5.2. Experimental

5.2.1. Materials and reagents

In this study sand (rounded form, silica content of 99%, water content < 0.1%) was used as obtained from Joomunjin silica sand company (South Korea). Heavy and light crude oils were received from Advanced Petroleum Technology Lab, Energy R&D Center, SK innovation Global Technology (South Korea). Characteristics of crude oils are indicated in Table 5.1.

Table 5.1. Characteristics of crude oils in the study

Characteristics	Light crude oil Kuwait	Heavy Crude Oil Bitumen
Viscosity, cSt at 20℃	-	> 50,000
Viscosity, cSt at 37.8℃	11.34	-
Viscosity, cSt at 50℃	7.74	-
Specific gravity (60/60F)	0.8729	1.0143
Gravity degree API	30.6	8
Compositions		
LPG, Naphtha	23.28	0
Distillate	26.47	14
VGO	25.8	34
VR	24.45	52
Sulfur, wt %	2.67	4.5
TAN, mg KOH/g	0.21	3.5

The chemicals including aluminum (Al^{3+} in $Al_2(SO_4)_3$, 98%), sodium sulfate anhydrous (Na_2SO_4, 99%), and n-hexane ($CH_3(CH_2)_4CH_3$, 95%); reference oil consisting of n-hexadecane ($CH_3(CH_2)_{14}CH_3$, 99%), isooctane, $(CH_3)_3CCH_2CH(CH_3)_2$, 99.8%), chlorobenzene (C_6H_5Cl, 99.7%); and tetrachloroethylene (C_2Cl_4, 99%) were purchased from Daejung Chemicals & Metals (South Korea).

5.2.2. Experimental setup

Oil-sand media was prepared by adding 50 mL of crude oil in 500 mL sand. The flocculation process was applied to create homogeneity in the reactor. Oil-sand media (500 mL) with water content of ~ 65% and pH of ~ 8.32 was placed in an acrylic cylinder reactor (D x H = 150 mm x 300 mm). Initial TPH concentration of prepared samples was about 4,800 mg/kg.

In set 1, different washing reagents, i.e. tap water, tap water and air, tap water and alum (2 mM), and NB were injected into the sample from the bottom of the reactor, as shown in Figure 5.1. The pressure of the washing reagents was 3.5 atm. and the wastewater was discharged from reactor after 10 min of treatment.

In set 2, the process of NB was carried out under conditions: pressure = 3.5 atm.; zeta potentials = ~ -12, ~ 0, ~ +15, and ~ +20 mV; NB/oil-sand ratio = 1/1, 2/1, 3/1, 4/1, and 5/1; treatment time = 10, 20, 30, and 40 min; injection

regime: batch and intermittent (at 5-min increments); types of NB: NB only and NB combined with ultrasonic sound. Control experiments for oil-sand separation by using water and Al^{3+} (at concentration of 0, 0.5, 1, and 2 mg/L) were also conducted at the same conditions as the NB processes.

After injection of NB into oil-sand reactor, pH of the fluidization was ~ 6.54 and was maintained during separation process.

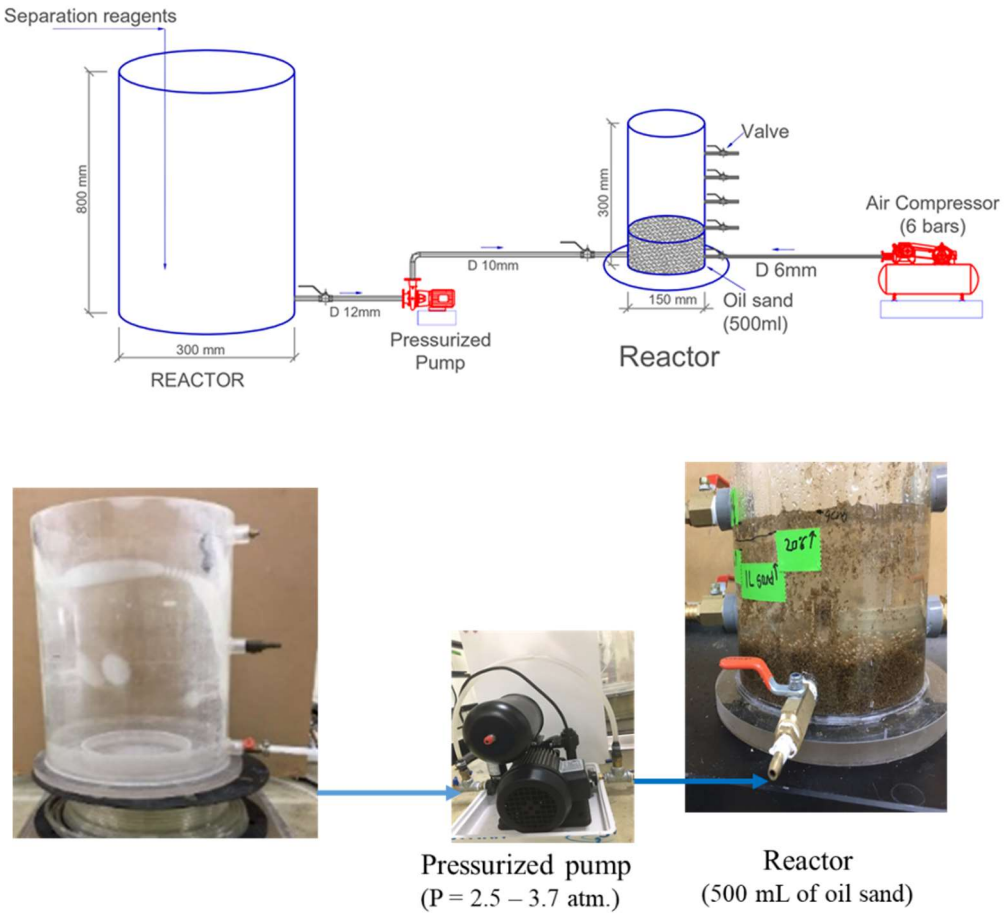

Figure 5.1. Schematic of oil-sand separation experiments

Zeta potential and average size of initial NB were measured by using zeta potential – particle size analyzer (ELSZ 1000, Japan). Table 5.2 summarizes the magnitude of NB zeta potential in dependence with concentration of Al^{3+} addition.

Table 5.2. Zeta potential values of NB in accordance with Al^{3+} concentration

Zeta potential of NB		Al^{3+} concentration (mM)
Negatively charged	-12 mV	0
Non-charged	~ 0 mV	0.5
Positively charged	+15 mV	1
	+20 mV	≥ 2

Bubbles coalescence, bubble-oil attachment, and oil-sand morphology were captured and analyzed with a system of microscopy (Sometech, Korea, magnification range from x1200 to x2400) and image analysis software (IT4 Plus); in addition, size distribution of the sand, oil-sand was measured by using Mastersizer 3000 (Malvern Instrument Ltd, UK); to observe the oil-sand profile after applying NB technologies.

Total petroleum hydrocarbon was extracted by adding 20 g of oil-sand with water content ≥ 60% into 100 mL of n-hexane beakers containing 10 g Na_2SO_4. After mixing at 300 rpm in 10 min, the mixture was filtrated with a syringe filter (diameter 28 mm, pore size 0.45 µm). The extraction process is indicated in Figure 5.2. The n-hexane extracted layer was transferred in a 2 mL GC vial and TPH was then measured by using Agilent GC system (model 7890B GC).

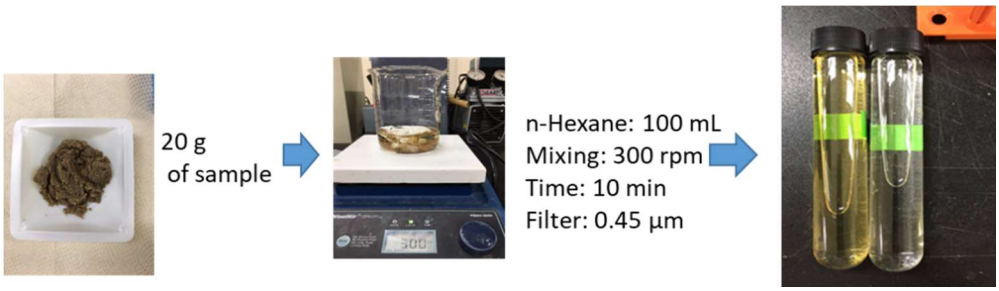

Figure 5.2. Extraction of TPH in n-hexane solvent

5.2.3. Method validation

Reference oil was prepared from 15 mL of n-hexadecane, 15 mL of isooctane, and 10 mL of chlorobenzene into stoppered 100 mL volumetric flask. Stock standard solution of 20,000 µL/mL was obtained from diluting 2 mL of reference oil in 100 mL of tetrachloroethylene. Calibrations were constructed with common concentrations of 0, 500, 1000, 2000, 5000, 10000, and 20000 µL/mL. Quantification of TPH was achieved from plotting peak

area of the chromatogram versus nominal concentration of the calibrations. A provided TPH was determined from analysis of every 2 samples in duplicate.

5.3. Bubble coalescence in oil-sand reactor

Figure 5.3 shows that bubbles were in micro-sized after injecting NB (~ 550 nm) into oil-sand fluidization. It was expected that the stream flow of bubble and solid surface in the oil-sand reactor will give an extreme force; in addition, oil acts as a surfactant; so that the NB can be coalesced to form large bubbles (micro and macrobubbles). Figure 5.3 also indicates the external contact angle (α) between the bubble and oil layer; that could be determined based on the bubble shape uniformity. In the oil-sand reactor, bubbles were mostly in spherical-like shape (oval and sphereical), as provided in figure 5.4; therefore the external contact angle would be measured by the normal and tangent lines at the contact point. As seen in figure 5.3, a large α (c.a. ~105^{o}, microbubbles of ~ 26.6 μm) creates a strong attachment between bubble and oil layer; meanwhile in case of a small α (c.a. ~ 38^{o}) the bubble (~ 44.8 μm) is weakly attached on the oil layer. Similar trend was reported by (Lim 2016), confirming that exponentially decrease in external contact angle enhances the NB coalescence to form greater microbubbles, as shown in figure 5.5.

Figure 5.6 illustrates the effect of treatment time on DO concentration (left panel) and bubble average size (right panel) for the positive and negative

bubbles. The data show that longer treatment time resulted in larger microbubbles and lower DO concentration. As seen in Figure 5.6, positive bubbles grew the size from ~ 32.1 µm (DO ≈ 16.72 mg/L) to ~1442 µm (DO ≈ 8.8 mg/L) after 40 min of separation; meanwhile negative bubbles had the size of ~ 17.4 µm after injection into the oil-sand reactor and of ~1109 µm after 40 min. In the present study, kinetic of DO and bubbles size relationship followed the equation (5.1) with $R^2 = 0.9963$, as given below.

$$y = k_1 \times C^2 + k_2 \times C + A \qquad (5.1)$$

Where y is average size of bubbles (µm); x is DO concentration (mg/L); k_1 (= 17.797), k_2 (= 636.75), and A (= 5700) are obtained from experimental results. Mechanism related to size change of bubbles in the oil-sand fluidization was attributed to coalescence phenomenon. It is expected that positive bubbles resulted in better coalescence; given by the size growth during treatment time of 40 min. Figure 5.7 shows that microbubbles came in contact to increase its size. As reported in previous study, bubble coalescence occurred in a rapid evolution (Bui 2019) or milliseconds (Kracht 2009); and in this study, 5 microbubbles in the size range of 10.5 ~ 25 µm coalesced to form a larger microbubbles of 28.4 µm in 0.005 s. Also, it was seen that movement only obtained with the bubbles that were not attached on the oil layer; moreover, bubbles with stronger attachment or larger size would greatly

attract ambient bubbles to achieve the coalescence. It was demonstrated that solid particles enhance the coalescence of the bubble (Ferreira 2017) and in this study, the presence of $Al(OH)_{3s}$ at pH > 4 is expected to result better coalescence for positive NB injection.

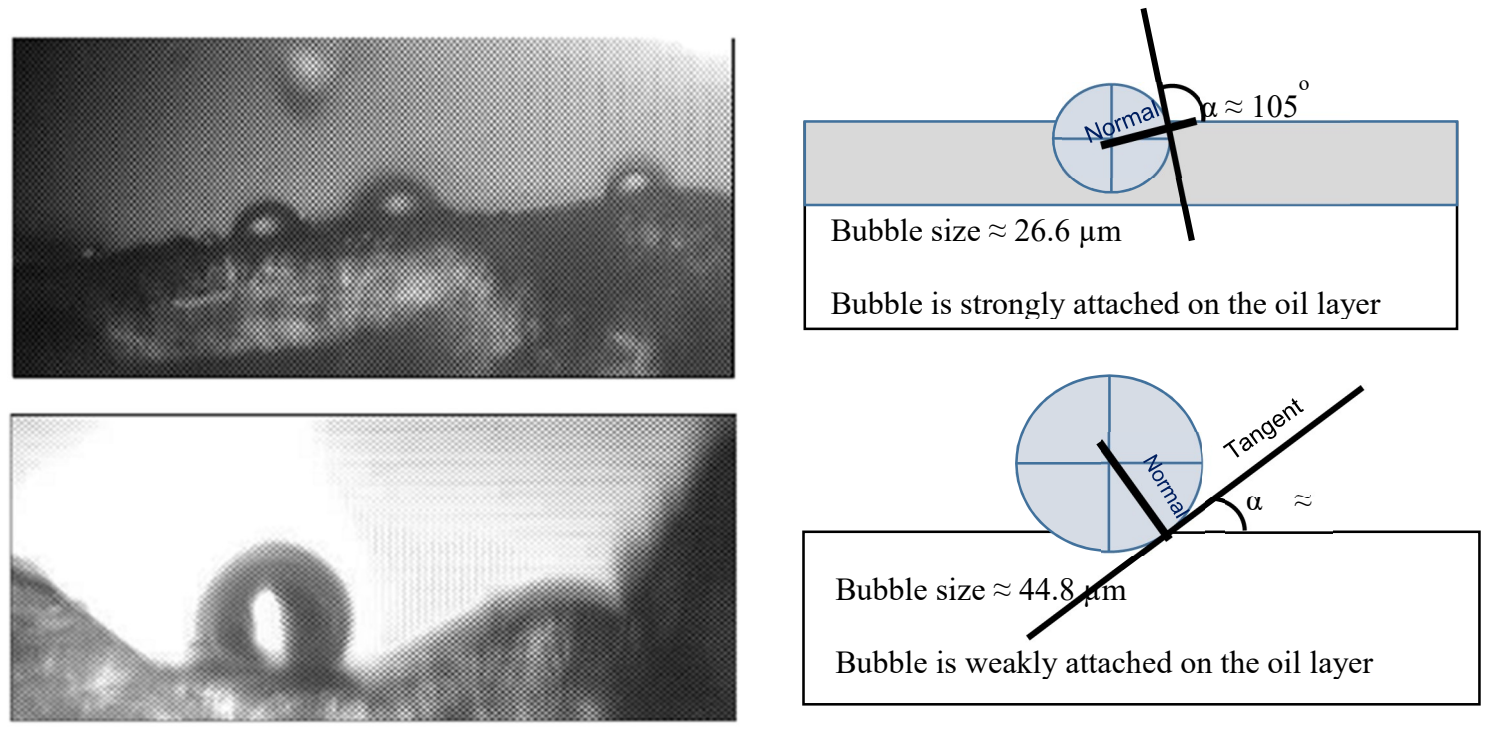

Figure 5.3. Attachment of bubbles on oil-sand media

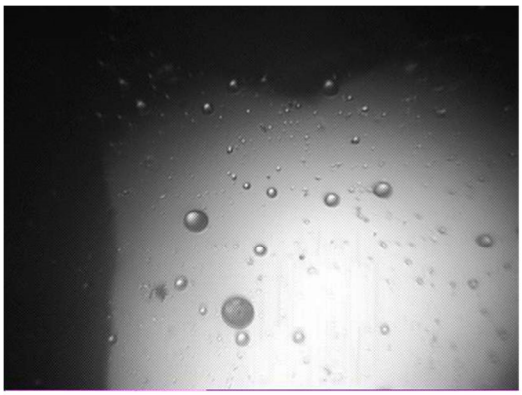

Microscope (Sometech, X1200)

Microscope (Sometech, X100)

Figure 5.4. Bubble shape uniformity in the oil-sand reactor (obtained from microscope, Sometech Ltd. Co., Korea)

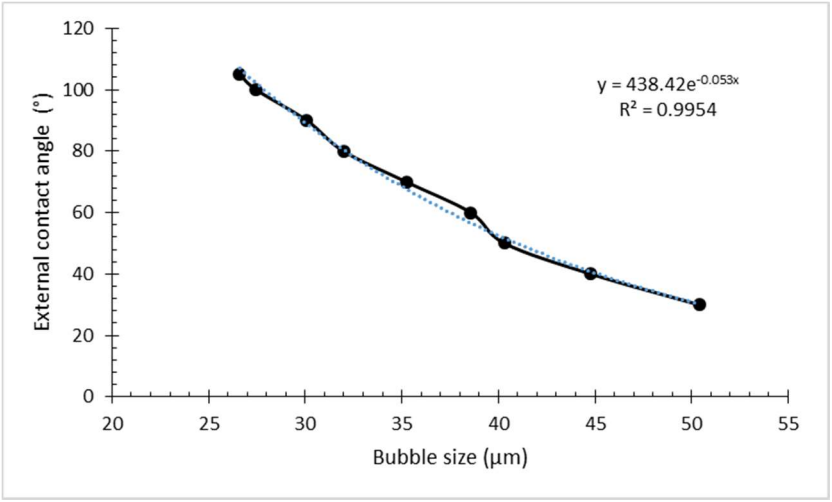

Figure 5.5. External contact angle of bubble on oil layer with respect to bubble size

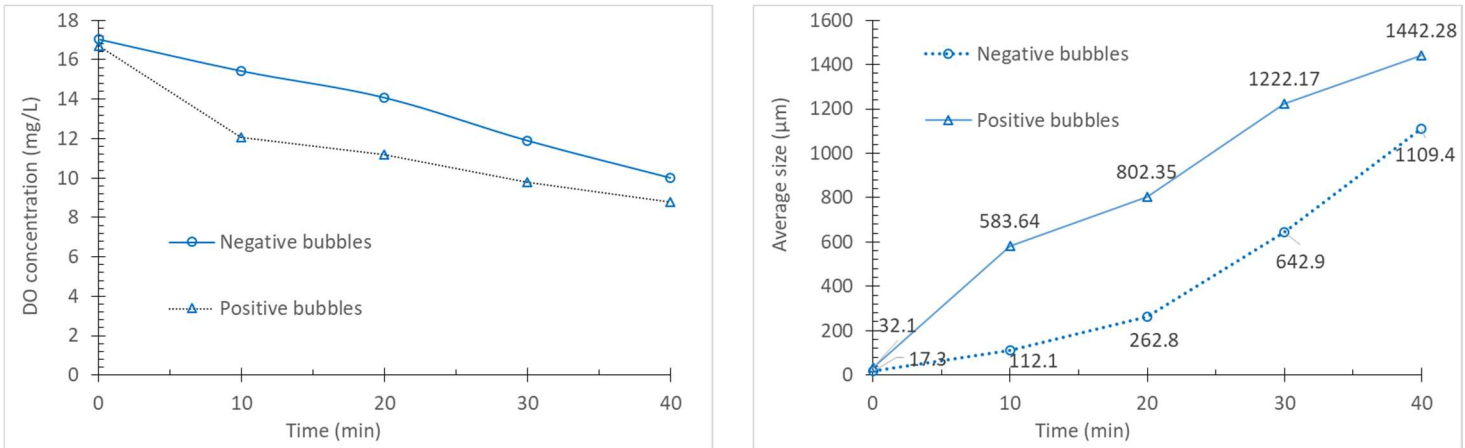

Figure 5.6. Temporal change in DO concentration (left panel) and bubble size (right panel)

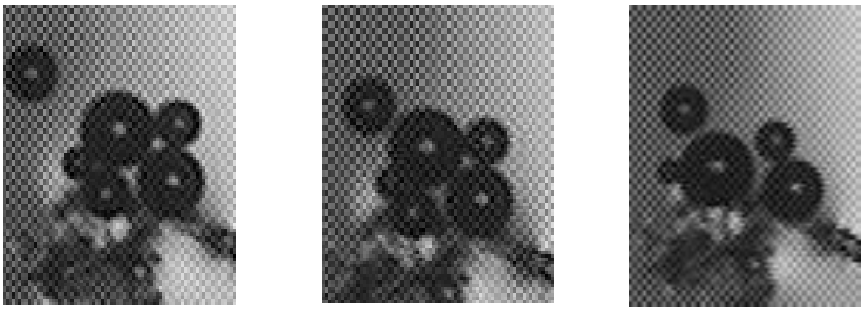

T T + 0.001 (s) T + 0.002 (s)

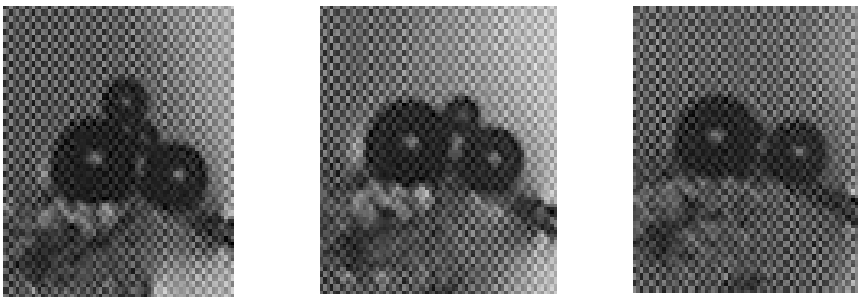

T + 0.003 (s) T + 0.004 (s) T + 0.005 (s)

Figure 5.7. Bubbles coalescence in oil-sand reactor

5.4. TPH removal efficiency

5.4.1. In different separation processes

Figure 5.8 shows TPH removal of heavy and light crude oil-sand using different washing waters; i.e. tap water, tap water and air, tap water and Al^{3+}, and charged bubbly water. It is obvious that all washing waters were more efficient in separating light oil (density of 0.876 g/cm^3) in comparison with heavy oil (density of 1.091 g/cm^3) from contaminated sand, confirming that

the density of the crude oil affected the efficacy of the washing water (density ≤ 1 g/cm^3).

In case of light oil-sand, the positively charged NB provided the greatest TPH removal (~ 70%); followed by the presence of tap water and air (~ 62%), negatively charged NB (~ 58%), tap water and Al^{3+} (~ 50%), and tap water only (~48%). As washing waters inserted into the reactor were pressurized, the formation of fluidization in the oil-sand media was obtained and the net forces acting on the oil-sand; i.e. interfacial forces (sand-oil, oil-bubbles, oil-water) (Tansel 2017), buoyancy force and shear (hydrodynamic) force (Kim 2012); was sufficient to drag oil on to the surface. In case of tap water only, the oil-water interaction was suggested as possible reasons for elevating TPH in oil-sand fluidization. Similar to backwashing process, the force of water actually lifted the oil-sand bed; however, this force could not detach oil from media bed efficiently. The addition of Al^{3+} could not accelerate the trapping of the oil-water attachment, resulting in similar TPH removal. Inducing air at the pressure of 6 atm; that could produce macrobubble to swirl oil-sand bed and enhance the oil-water, oil-air, oil-macrobubble interactions by hydrodynamic force; improved separation efficiency.

Bubble coalescence forces and hydrodynamic (shear) force from injection of the NB into the oil-sand reactor were expected for better TPH removal.

(Lim 2018) demonstrated that coalescence of the bubbles improved its attachment probability and strength on the oil layer. Also, in many systems, microbubble clusters attached randomly on the oil layer to increase surface area on the attachment (Kim 2012, Lim 2015, Lim 2016, Lim 2018). In this present study, the increase in TPH removal from the presence of positive NB was due to better coalescence in the bulk solution (Temesgen 2017, Bui 2019), that could increase bubble-oil attachment force, as compared to negative NB' presence.

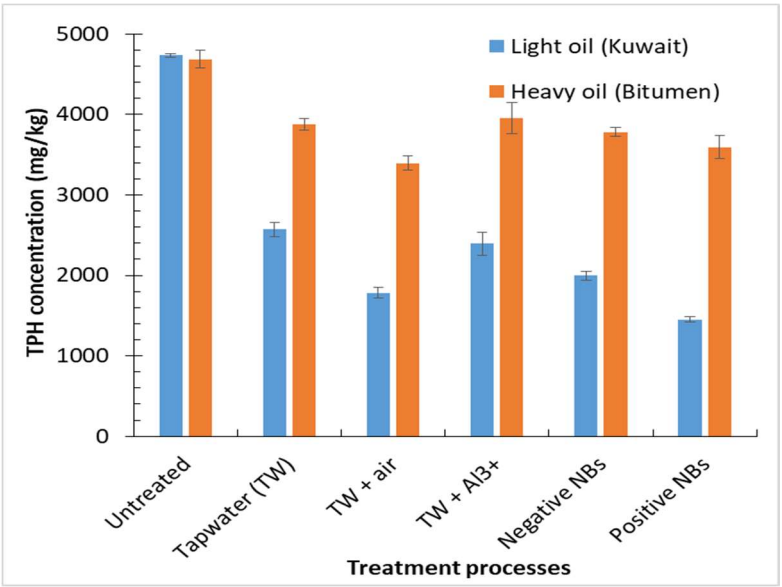

Figure 5.8. Separation of crude oil-sand in different treatment processes

As can be observed from Figure 5.9 – left panel, a floated layer was resulted in the presence of bubbly waters (both negative and positive bubbles). Our results obtained from microscopic analysis showed various attachment

positions of bubbles on the oil-sand grains (Figure 5.9 – right panel). It was seen that bubbles were strongly attached onto a single oil-sand particle or tightly arranged on multiple oil-sand grains. The net force, F_n, necessary for detachment of the oil-sand was the difference amongst buoyancy force, shear force from bubbles, and interfacial force between oil and sand as followings:

$$F_n = F_s + F_f - F_b \qquad (5.2)$$

Where F_s was shear force from NB injection process, F_f was sum of buoyancy force of bubbles, and F_b was interfacial force between oil and sand. To release oil from the media bed, F_n must be > 0; that means sum of F_s and F_f were greater than F_b. Our discussion was in an excellent agreement with a conclusion in a recent research (Tansel 2017). It was mentioned that the thin oil film could create little mobility of the sand due to the lubrication between particles; in addition, the floated bubble-oil layer was produced from negativity of net gravitational force (difference between the weight and buoyancy of the bubble and oil contaminants). In the oil-sand reactor, the NB coalesced to form microbubbles and macrobubbles, therefore it maintained the large surface and great buoyance force of the bubbles. In addition, the bubble-oil attachment was improved due to variety of bubble arrangement at the oil layer detach oil layer.

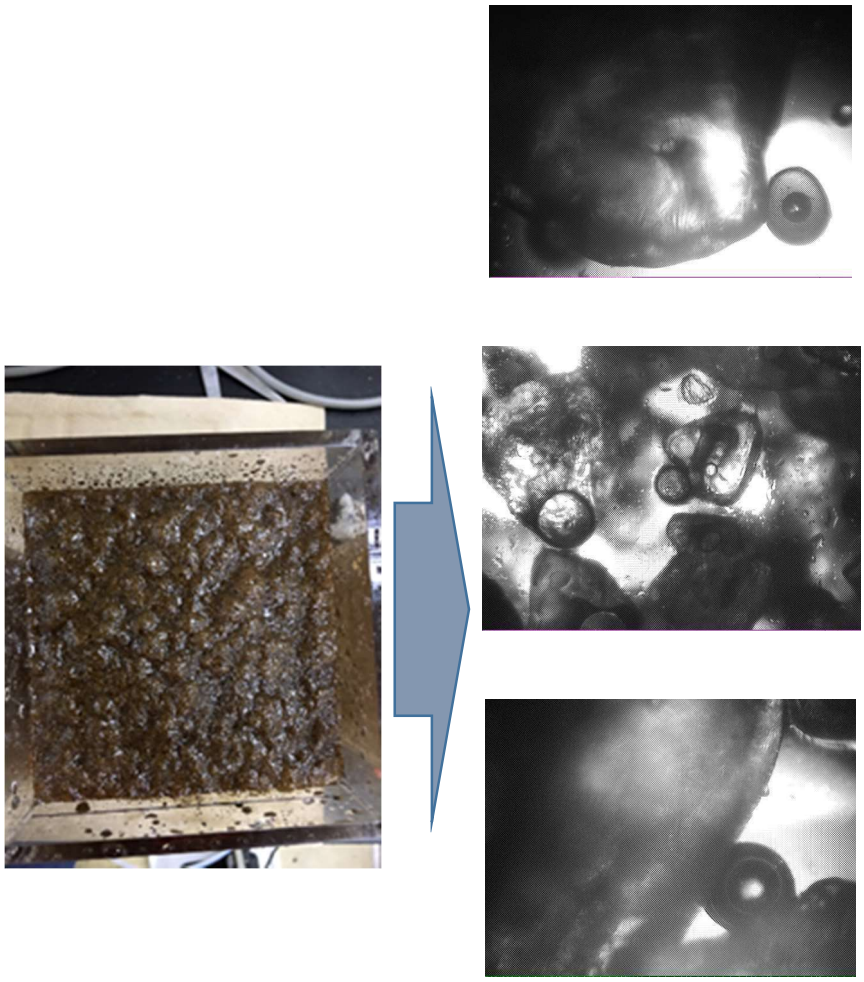

Figure 5.9. Microscopic analysis of floatable bubble-oil contaminated sand layer

5.4.2. Optimization of NB technologies for oil-sand separation

5.4.2.1 Effect of NB/oil-sand

Figure 5.10 summarizes the TPH removal efficiency at various NB zeta potentials (ca. –12, 0, +15, and +20 mV) with respect to ratio of the NB and the oil-sand. In all cases of control experiments, better TPH removal rate was obtained at water (with or without Al^{3+})/oil-sand of 5/1. As observed, the lowest TPH removal efficiency of approximately 50% achieved at the NB/oil-sand of 5/1 in non-charged NB application. Oil-sand detachment efficiency increased by approximately 75% at NB/oil-sand of ≥ 3/1 and >86% at NB/oil-sand of ≥ 2/1 in the injection of negatively and positively charged NB, respectively. The greater TPH removal and lower NB/oil-sand ratio indicate that the attachment force between oil layer and the charged bubbles were stronger, as compared to the non-charged bubbles. These results confirm that using positive NB that resulted in greater attachment between bubble and oil layer required the smallest bubble volume concentration injected into the oil-sand bed. Surface charge also affected the optimal amount of initial NB inserted to oil-sand bed, with following order: positive NB < negative NB < non-charged NB. However, due to the use of n-hexane to extract the oil from the sample, it was difficult to observe the oil's surface charge. Therefore, discussion on the effects of bubble's surface charge on NB/oil-sand ratio for

maximum TPH removal is still challenging. In this work, we found that positive NB technology allows to minimize the required washing bubbly water volume to detach oil from the oil-sand.

5.4.2.2. Effect of separation time

Figure 5.11 indicates the TPH removal of the oil-sand by NB technologies with respect to treatment time. In control experiments, better TPH removal was obtained in the presence of Al^{3+}; however, [Al^{3+}] had little effect on decreasing treatment time, indicating the treatment time of 40 min.

Overall, the treatment time insignificantly improved the TPH removal in case of positive NB. As seen, the excellent TPH removal efficiency (~ 90%) was achieved and maintained from the first 10 min and 20 min in the application of NB with zeta potential of + 20 mV and +15 mV, respectively (Figure 5.11). In contrast, TPH removal in the injection of non-charged and negatively charged NB was improved with increase in the treatment time. The experimental results showed that approximately 54 %, and 80% of TPH were removed at 40 min in such systems.

In positive NB process, the rising velocity of coalesced bubbles is expected to significantly impact the separation time. The increase in bubble rising velocity (due to the coalescence of positive bubbles for larger bubble formation) could produce stronger buoyancy force and the bubble-oil (sand)

attachment floated in shorter time. In addition, greater positive zeta potential value could decrease separation time; confirming that positivity of the NB zeta potential affected oil-sand separation performance.

The increase in separation time with non-charged and negatively charged NB technologies evidenced that the coalescence of these bubbles required a certain time to create the sufficient buoyancy force. Also, the longer treatment time may be related to the interaction kinetic of the negatively charged and non-charged bubbles and oil-sand bed vs. the contact time. In particular, the data from Figure 5.11 show that kinetics of TPH removal from oil-sand followed by given below equation.

$$\ln C = \ln C_0 - kt \qquad (5.3)$$

Where C and C_0 were residual and initial concentration of TPH (mg/kg), respectively; k was rate constant (min^{-1}), and t was separation time (min). Based on experimental results, rate constants for TPH removal by negatively charged and non-charged NB processes were k_{neg}= 0.0562 min^{-1} and k_{non} = 0.0342 min^{-1}, respectively. At the same separation time, greater rate constant value resulted in better TPH removal efficiency; i.e. injection of negative NB with k_{neg} led the separation time of 40 min with a TPH removal of ~80%; meanwhile, k_{non} of the process using non-charged NB obtained an efficiency of ~54%. The observation of rate constant demonstrates that the processes

carried out using negatively charged NB generally were more feasible in the separation of the oil from contaminated sand.

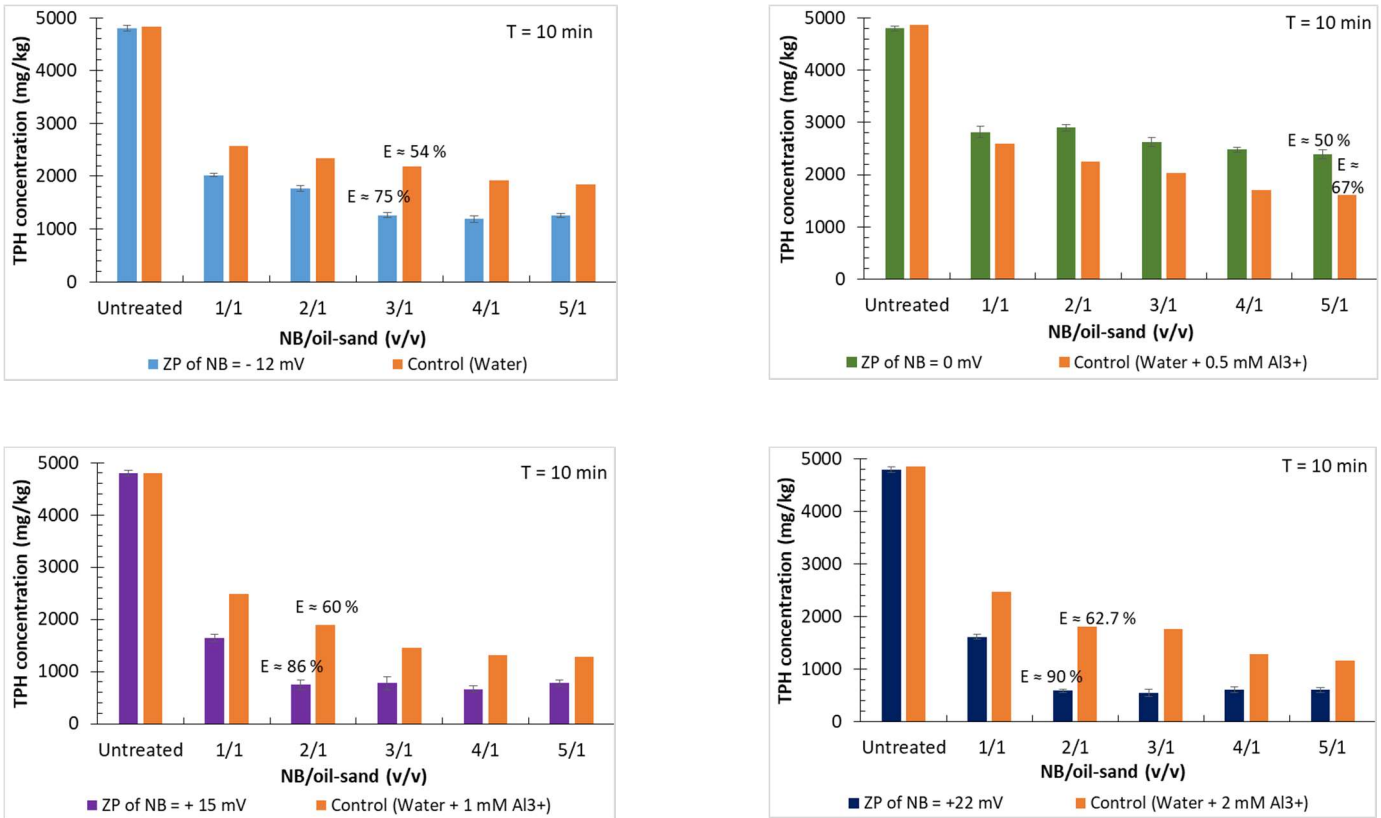

Figure 5.10. Effect of NB/oil-sand on TPH removal

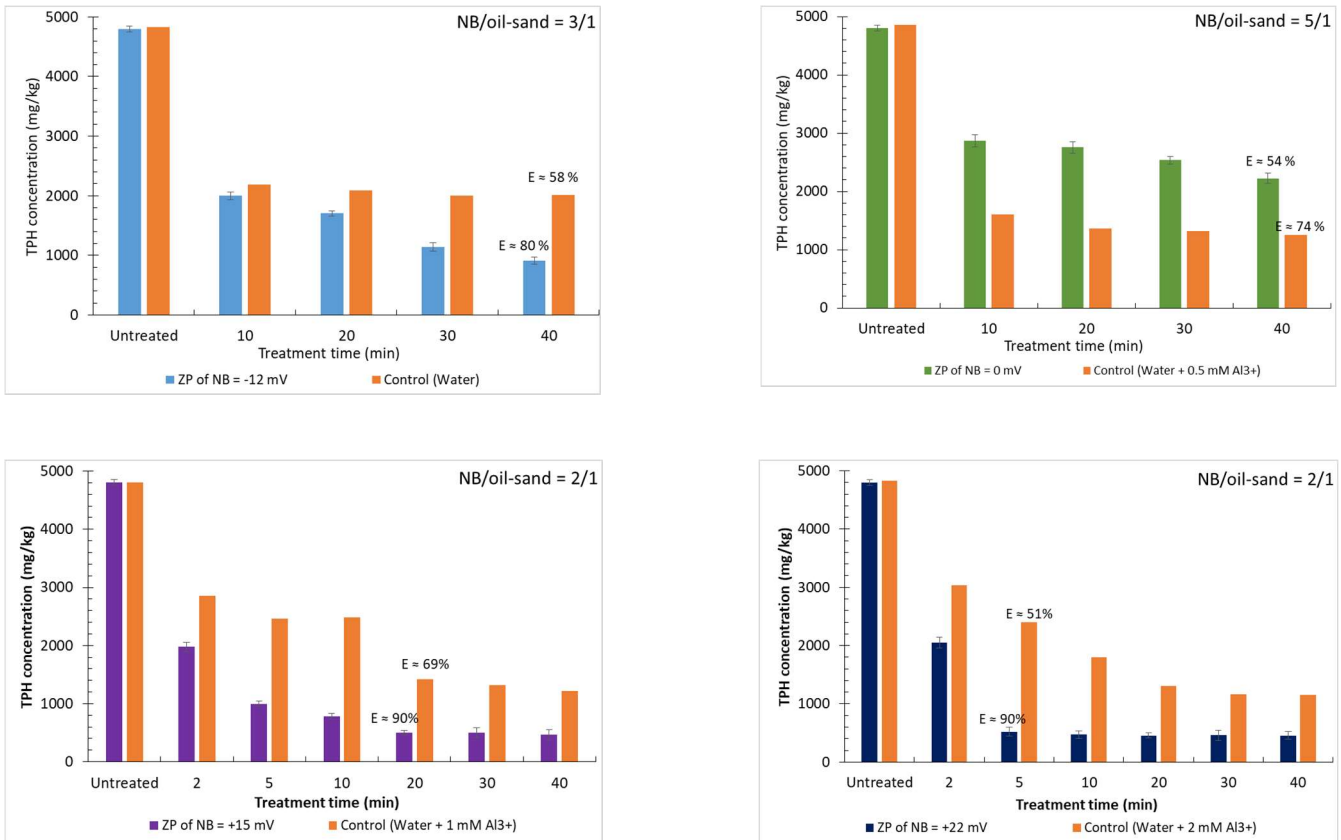

Figure 5.11. Effects of treatment time on TPH removal

5.4.2.3. Effect of NB injection

Oil-sand separation performance with respect to batch and intermittent NB injection was carried out under conditions: NB/oil-sand = 3/1 (ZP = -12 mV), 5/1 (ZP = 0 mV), and 2/1 (ZP = +15 and +20 mV); treatment time = 40 min (ZP = -12 and 0 mV), 20 min (ZP = +15 mV), and 10 min (ZP = +20 mV). Overall, negatively charged and non-charged NB processes showed similar results in TPH removal efficiency from both NB injection regimes; meanwhile, TPH removal in positive NB process were obtained the removal of ~94% and ~85% for intermittent and batch injection, respectively. As positive NB were inserted intermittently, the coalescence were improved and obtained in sequential; therefore, the transfer from bubbly regime to bubble-oil aggregate regime was also enhanced. However, the positively charged NB process with intermittent injection regime increased operation time and the coalescence of positive bubbles trended to form larger microbubbles and/or macrobubbles; therefore, three scenarios of attachment could be observed in this regime: microbubble-oil (sand), macrobubble-oil (sand), and microbubble-macrobubble-oil (sand). Previous works demonstrated the high probability of mirobubbles attached on to oil layer and the improvement of the attachment between macrobubbles and the oil layer (Ahmadi 2014, Lim 2018). According to results reported by (Lim 2018), the attachment time of

macrobubble-oil decreased by 82% in comparison with that of microbubble-oil; confirming that during operation time coalesced bubbles would greatly attach on the oil (sand) layer to release the oil from media bed.

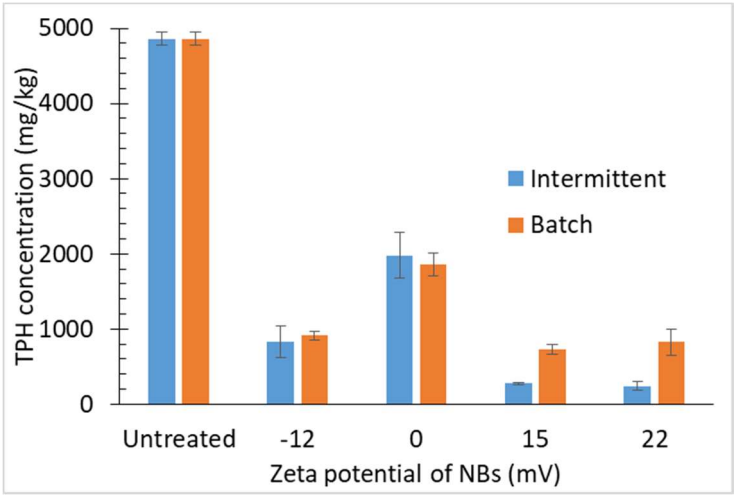

Figure 5.12. Effect of NB injection regime on TPH removal

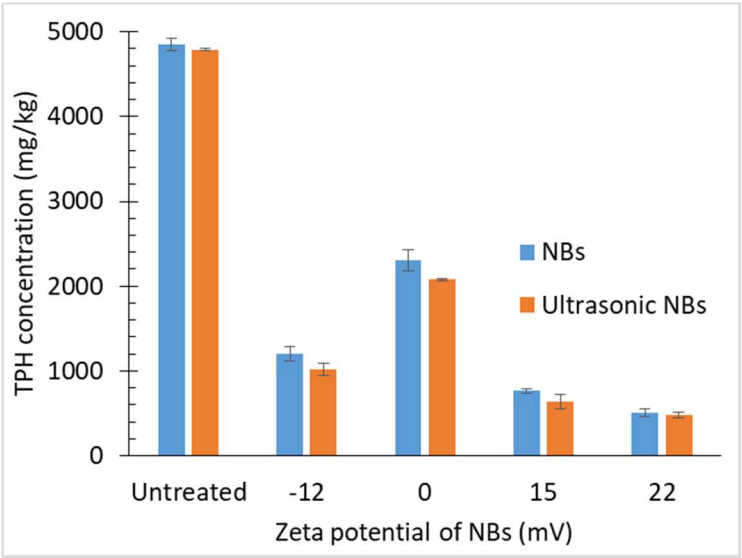

Figure 5.13. Effect of NB and ultrasonic NB on TPH removal

Now considering separation performance of the oil-sand in the presence of the NB alone and NB combined with ultrasonic sound. In this experimental set up, the NB were first inserted in to the oil-sand reactor and ultrasonic was then applied. There was insignificant difference in TPH removal with the efficiencies of ~ 75% for negative NB, ~56% for non-charged NB, and ~ 90% for positive NB in both cases (Figure 5.13). These results imply that the effects of ultrasonic sound could be negligible in the removal of TPH by the NB processes. As discussed earlier in this work, initial NB shifted to microbubbles after inserting in to the oil-sand fluidization; thus, the ultrasonic sound seemed not to enhance the microbubbles-microbubbles attachment and not to increase the bubble rising velocity. With this respect, the strength of bubble-oil (sand) attachment and the buoyancy force of these aggregates in both separation processes were similar to obtain similar TPH removal.

5.4.3. Change of the oil-sand morphology using NB technologies

Figure 5.14 shows the size distribution of the raw sand and the treated oil-sand by the NB processes. Overall, about 93% of the raw sand ranged in the size from ~ 300 μm to ~ 1110 μm and the size arrangement of the oil-sand was larger, ca. ~ 270 to ~ 1260 μm. Interestingly, the treated oil-sand by positive NB process had similar size profile to the raw sand with the fraction of the particles of ~ 20% from 400 to 450 μm and ~ 70% from 450 to 800 μm (Figure

5.14). In the application of the non-charged NB the fraction of the particles in the treated samples was most likely to that of the untreated oil-sand. According to Figure 5.12, particle sizes of the oil-sand after negative NB technology were allocated identically as more than 85% of the particles was from 400 to 750 µm.

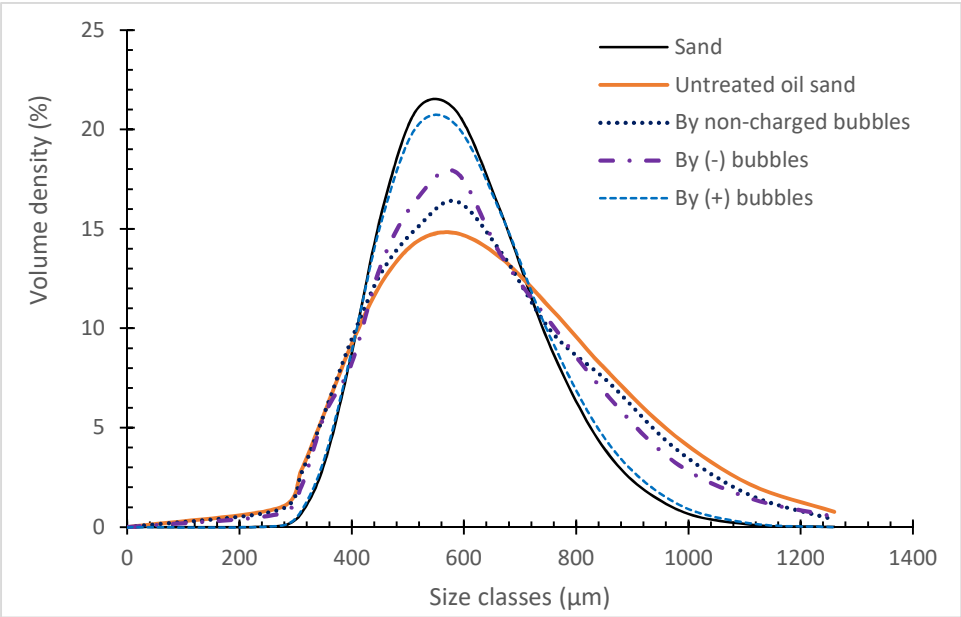

Figure 5.14. Size distribution of the oil-sand in NB processes

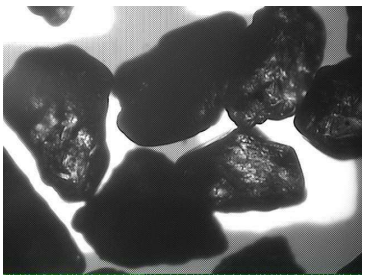

a) Raw sand

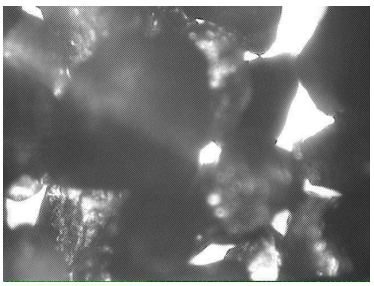

b) Untreated oil-sand

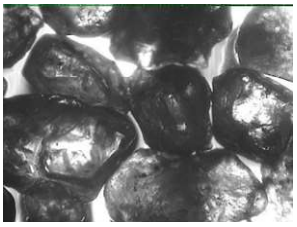

c) After negatively charged bubbles technology

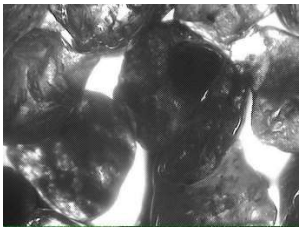

d) After non-charged bubbles technology

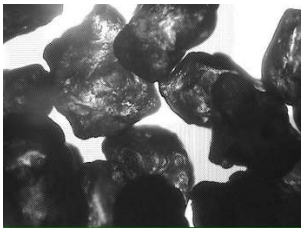

e) After positively charged bubbles technology

Figure 5.15. Microscopic observation of the sand and oil-sand morphology

In Figure 5.15, the morphology of the sand and oil-sand was obtained from microscopic observation. Based on our observation, the morphology of the oil-sand after injecting positive NB was closely to that of the raw sand, followed by that of the oil-sand after the negative and non-charged NB processes, respectively. Microscopic data provided a visual evidence about the separation of the oil from the contaminated sand before and after applying NB technology. Our observation results supported the discussions on the effects of the NB processes with respect to the zeta potential on the TPH removal efficiency; confirming that positive NB drove the better oil-sand separation

performance. However, the application of negative NB could also be an efficient tool in the field of oil-sand detachment.

5.5. Summary

In this chapter, the application of the NB processes for the oil-sand was demonstrated to be efficient techniques. Separation performance was affected by the NB/oil-sand ratio, treatment time, and NB injection (i.e. batch and intermittent regimes). It was shown that the NB and ultrasonic application insignificant improved the TPH removal from the oil-sand. As resulted, the injection of intermittent NB with positive zeta potential, the NB/oil-sand ratio of 2/1 and the treatment time less than 20 min provided the higher TPH removal efficiency. It was also found that stronger buoyancy force resulted from bubble coalescence enhance the separation efficiency. In summary, positively charged NB technology is the most effective for the oil-sand separation.

References

Ahmadi, R., Khodadadi, D.A., Abdollahy, M., Fan, M. (2014). "Nano-microbubble flotation of fine and ultrafine chalcopyrite particles." International Journal of Mining Science and Technology 24(4): 559-566.

Bui, T., T., Nguyen, D., C., Han, M., Y. (2019). "Average size and zeta potential of nanobubble in different reagent solutions." Journal of Nanoparticle Research 21(8).

Kim, T. I., Kim, Y. H., Han, M. Y. (2012). "Development of novel oil washing process using bubble potential energy." Marine Pollution Bulletin 64(11): 2325-2332.

Kracht, W., Finch, J., A. (2009). "Using sound to study bubble coalescence." Journal of Colloid and Interface Science 332: 237-245.

Lim, M., W., Lau, E., V., Poh, P., E. (2018). "Micro-macrobubbles interactions and its application inflotation technologyfor the recovery of high density oil from contaminated sands." Journal of Petroleum Science and Engineering 161: 29-37.

Lim, M., W., Lau, E., V., Poh, P., E. (2016). "Analysis of attachment process of bubbles to high-density oil: Influence of bubble size and water chemistry." Journal of the Taiwan Institute of Chemical Engineers 68: 192-200.

Lim, M., W., Lau, E., V., Poh, P., E., Chong, W., T. (2015). "Interaction studies between high-density oil and sand particles in oil flotation technology." Journal of Petroleum Science and Engineering 131: 114-121.

Tansel, B., Boglaienko, D. (2017). "Self assembly, mobilization, andflotation of crude oil contaminated sandparticles as granular shells on gas bubbles in water." Science of the Total Environmentjournal 574: 437-442.

Temesgen, T., Bui, T. T., Han, M. Y., Kim, T.-I., Park, H. J. (2017). "Micro and nanobubble technologies as a new horizon for water-treatment techniques: A review." Advances in Colloid and Interface Science 246: 40-51.

CHAPTER 6. CONCLUSIONS AND RECOMMENDATIONS

6.1. Conclusions

This study investigates the generation of positively charged NB and its applications for color removal and oil-sand separation. Controlling zeta potential of the NB significantly affects the treatment efficiency. Reactive species generation in the NB processes allows it to be feasible for color removal. Moreover, wide applications of the NB for particle separation, especially oil remediation from the contaminated sand, have been anticipated via the high floatability of the bubble-particle aggregates.

The formation of NB were carried out by collapsing of the microbubbles in the Teflon hose. The generated bubbles had average size of ~ 500 nm, confirming the success of the NB creation. The NB size had no dependency on the solution pH and grew over time. Coalescence of NB was the proposed mechanism of the size growth. Positive NB were resulted in the presence of cationic surfactant (DODAB) and tri-valence metal ions (Al^{3+} and Fe^{3+}). The zeta potential of the NB decreased at more alkaline pH and remained over time of 150 min. The adsorption of the positive species and hydroxide precipitates was expected to mainly create positive NB in such solutions.

Considering the effects of the most widely-used coagulant such as Al^{3+}, it was found that the concentration of Al^{3+} had no effect on the NB size but it played the major role on changing the ZP magnitude. Specifically, zeta potential of the NB charged negatively (~ -12 mV) in the absence of Al^{3+}, neutrally in the addition of 0.5 mM Al^{3+}, and positively (ca. ~ +15 to ~ +20 mV) in the presence of Al^{3+} (i.e. concentration from 1 to 2 mM, respectively). These results also demonstrated that the NB (negatively charged, non-charged, and positively charged) was stable during 150 min of the observation; evidencing that stability of the NB in the Al^{3+}-solution. This finding allows the use of the Al^{3+} in formation of the NB for its further applications in the environmental processes.

The decolorization of Rit dye by NB technologies, especially in the presence of ultrasonic NB and NB/H_2O_2, was demonstrated to be an efficient treatment process. We found that NB ZPs and reactive species such as $OH^{\cdot}$, $HO_2^{\cdot}$, and $O_2^{\cdot}$ were fundamental for Rit dye decolorization significantly by the NB-based processes. In particular, a weaker color (~500 CU) resulted in a higher decolorization rate, with the requirement of a shorter treatment time and lower positive ZPs of NB applied, in comparison with a stronger color (~1200 CU). In the present study, reaction mechanisms follow two possible paths such as electrostatic attraction (i.e. opposite surface charge) and the oxidation (i.e. reactive species) have been found to drive decolorization of Rit

dye in the NB systems. The decolorization time in the NB processes depended on the rising velocity of the bubbles, the transfer from the bubbly regime to aggregate regime, and the reaction kinetics of the reactive species and Rit dye molecules. Overall, the NB technique is promising to separate the color from polluted water because of the surface charge attraction between bubbles and dyes and the excellent oxidation by the reactive species.

Separation of the oil-sand using NB technology was shown to be an effective treatment process. Several factors such as the NB/oil-sand ratio, separation time, and NB injection regime (i.e. batch and intermittent) were demonstrated to significantly impact the separation performance (assessed by TPH removal); whereas, the NB combined with ultrasonic sound was negligible to enhance the oil remediation from the contaminated sand. It was concluded that the intermittent injection of the NB with the ZP from +15 mV to +20 mV, the NB/oil-sand ratio of 2/1, and the treatment time from 10 to 20 min resulted in the better TPH removal. Better coalescence obtained in the positive NB was attributed to create stronger buoyancy force; aiming at enhancing removal of TPH from the oil-sand.

6.2. Recommendation for further study

Physical properties of the NB such as size and zeta potential have been studied for recent decades; however, the studies on the applications of the NB

by controlling its zeta potential are still limited. With this respect, this research is in the line of the few studies on the use of the NB for water treatment and soil remediation. It is still a challenge to present the analysis of the NB mobility in the bulk solution; therefore more attention should be taken into account with the observation of the NB horizontal movement in the solution to provide more accurate zeta potential.

Rising velocity of the NB is shown as slow so that in the application for flotation the NB may require longer time; therefore further studies should modify this technique to aim at shortening the transfer from nanobubbly regime to bubble-particle aggregates. In a scenario, the NB would need some time for larger bubbles formation (via coalescence mechanism) to allow the flotation occurrence. It is thus recommended to carry extensive investigations of the coalescence for the NB, leading to apply more efficient NB technology in the field of the flotation.

Air NB in the combination with H_2O_2 or ultrasonic sound could accelerate the color removal in the water due to the oxidation. Furthermore, oxygen NB have been found to stay longer in the bulk solution and to own strong oxidation to discolor textile wastewater. A study on the effects of the air NB and oxygen NB on the decolorization performance should be done to provide more feasible NB technique, aiming at low cost and low energy consumption.

Considering the limitation of the NB in removing bitumen from the sand from this study, it is important to carry out more works on improving the efficiency by using the NB for heavy crude oil-sand separation. Investigation on the operational conditions, specifically the maintenance of NB size in the oil-sand reactor, should be focused to create integrated attachment between bubbles (nano, micro, and macro bubble) and oil layer; aiming at producing strong buoyance force that can exceed the friction force between heavy oil and the sand particles to improve the separation performance.

국문초록

나노버블 기술은 이론적으로 그리고 실험적으로 화학물질 소비가 적고 처리시설의 규모를 줄일 수 있는 경향이 있다고 알려져 있다. 따라서 설계 및 작동 비용 절감으로 인한 친환경적 기술로의 상당한 가능성을 가지고 있다. 이러한 관점에서 다양한 조건 하에서 수처리 및 물질 분리 공정을 위한 NB 기술이 연구되어 오고 있으며, 대부분의 경우 NB 표면 전하는 처리 효율에 연관된 주요 인자 중 하나이다. 따라서 이 연구는 양의 전하의 NB를 3가 금속이온(특히Al^3) 존재 하에서 발생시키고 이러한 NB를 색도 제거 및 기름-토양 분리에 적용하는 것에 집중하고 있다. 이 연구에서 NB는 믹싱챔버에서 과포화된 공기-물 혼합체가 퍼지면서 생성이 된다. 이는 그 후 테프론 호스에서 미세기포의 분해를 일으킨다. NB의 사이즈와 제타 전위는 동적광산란에 의해 측정이 되었다. 전반적으로 NB의 사이즈는 pH에 의한 경향이 없고 시간에 따라 커지며 여기서 사이즈 증가의 가능한 매커니즘은 용액 내에서의 응집과 연관이 되어있다.

양의 전하를 가진 NB는 화학적 시약의 존재 하에 관찰이 되며 특히Al^{3+} 는 수처리에서 가장 널리 사용되는 응집제이다. 양의 NB 생성은 양이온의 계면활성제(dimethyldioctadecylammonium bromide)의 존재 하에 확정이 되며, 3가 금속 이온의 추가로 만들어진다 (Al^{3+} and Fe^{3+}).

NB의 제타전위는 pH 2에서 12까지 증가하면서 모든 용액에서 감소한다. Al^{3+} 의 존재 하의 양의 NB는 특정 양이온 물질(pH<6 에서) 및 NB 표면의 수화물 침전(pH=6-9에서)에 의해 생성이 된다. Al^{3+} 의 양의 제타 전위 거동에의 영향이 아래의 조건에서 관찰이 되었다: $[Al^{3+}]$ 0에서 10mM 농도로 150분. 결과는 $[Al^{3+}]$는 NB의 사이즈에 거의 영향을 주지 않으며 NB의 제타전위는 0, 0.5, ≥ 1 mM 일때 각각 음으로 하전, 전하를 띠지 않고, 양으로 하전되었다. 최대의 제타 전위는 ≥ 2 mM Al^{3+}의 농도를 넣어주었을 때 +20 ± 2 mM였다. 모든 경우에 제타 전위는 150분 이후에는 유지가 되었으며 제타 전위 분석으로 NB의 안정성에 대한$[Al^{3+}]$의 현저하지 않은 영향에 대해 확인할 수 있었다. 이러한 관점에서$[Al^{3+}]$의 존재하의 양의 NB는 색도 제거 및 기름-모래 분리를 위한 처리 효율을 평가하는데 사용이 되었다.

색도 제거에 대한 실험적인 결과는 Al^{3+}만을 사용했을 때와 H_2O_2 만을 사용했을 때를 비교하기 위한 진초록색의 Rit 염색약의 색도 제거로 확인을 하였다. 그리고 양의 NB의 역할, NB만을, 초음파 NB, NB/H_2O_2를 사용했을 때 공정에서 색도제거 비율에 대한 반응성에 대해 확인하였다. Al^{3+}만을 사용했을 때와 H_2O_2 만을 사용했을 때 색도 제거 과정은 Rit dye가 500~1200 CU의 농도로 포함이 되어있는 칼럼 반응조의 바닥에 30%의 버블 비율로 기포 용액을 주입하여 자테스트를 하는 것으로 진행이 되었다.

모든 경우에 약한 색깔을 띨수록 색도 제거가 잘 되는 것을 보였다. 게다가 NB 시스템을 이용한 색도 제거가 기존의 방식을

사용하는 것 보다 효과적이었다. 두 염료 농도에서 양의 초음파 NB (제타 전위 +15mV에서 +20mV)와 양의 NB/H_2O_2 (1 mM) 시스템이 효과적인 처리 과정으로 판단이 되었다. 색도 제거의 매커니즘은 양의 NB와 염료 성분의 정전기식 인력 때문이다.

게다가 $OH^{\cdot}$, $HO_2^{\cdot}$, 그리고 $O_2^{\cdot}$ 의 반응기들은 초음파 NB와 NB/H_2O_2 시스템에서 Rit 염료의 저감능력 향상에 있어서 기본적이다. 90% 이상의 Rit 염료가 30분 이내에 제거가 되었으며, 초음파 NB와 NB/H_2O_2 계에서는 60분 후에 제거가 되었다. 다양한 NB의 존재하에 다른 색도 제거 시간이 기체상에서 응집물질 상으로 변환이 되는 것에 기여를 하였으며 반응기와 Rit 염료 성분의 반응 역학에 영향을 끼쳤다.

기름-모래 분리에의 적용에서 NB의 주입은 TPH 제거율 85% 이상으로 효과적인 처리 공정임이 밝혀졌다. 결과는 NB/기름-모래 비율, 분리 시간, NB주입(배치, 간헐적 반응)이 NB 공정으로 기름-모래 분리의 효율에 영향을 끼치는 것으로 드러났다. 초음파의 적용은 분리능력을 현저하게 향상시키지는 않는 것으로 드러났다. 결과적으로 2/1(v/v) 비율의 NB/기름-모래에서 양의 NB(제타전위 +15에서 +20mV)의 간헐적 주입이 높은 TPH 제거율을 얻을 수 있었다.

그러나, 음으로 하전된 NB 기술은 또한 높은 NB/기름-모래 비율과 긴 처리시간을 요구하지만 기름-모래 분리를 할만한 기술인 것으로 고려가 되었다. 부력이 기름을 떨어뜨리는데 주요한 역할을 하였다. 기포와 기름 층 사이의 큰 외부 접촉각이 기름-모래

반응조에서 NB의 응집으로 인한 미세기포와 매크로기포의 생성을 한다고 밝혀졌다. 그리고 기름층에 부착이 된 응결된 기포의 수의 증가는 더 나은 TPH의 제거를 위해 더 강한 부력을 생성하기에 필수적이라는 것을 알 수 있었다.

NB 공정은 오염된 물의 색도 제거와 기름-모래 제거를 위한 믿을만한 증거가 될 것이라는 것을 확인이 되었다. 두 분야 모두에서 NB의 제타전위 +20mV 값에서 최적의 처리 효율을 보인다는 결과를 얻을 수 있었다. Al^{3+}의 추가로 형성이 된 양의 NB를 사용하는 기술이 가장 효과적이라는 사실이 밝혀졌다. 이 연구에서의 발견은 수처리와 토양 완화를 위한 새로운 지평으로써 NB 기술의 더 나아간 적용을 말해준다.

주요어: 기포 응결, 기포 사이즈, 기포 제타 전위, 염료 색도제거, 정전기적 인력, 부상, 기름-모래 분리, 양으로 하전된 나노버블, 반응기

학번: 2016-37194

Acknowledgements

First and foremost I would like to thank Buddha for his supports, nourishments, and healings in my life.

I am always grateful to my supervisor Prof. Mooyoung Han, for his guidance, supports during my study period.

I am very grateful to the helps and supports from my lab members, especially Dr. Kim, Dr. Park, Dr. Tulinave, Dr. Dung, Dr. Canh, Dr. Tatek, Mr. Hyunwoo, Mr. Donggeun, Ms. Gippeum, Mr. Yusik, Ms. Saerom, Ms. Jooho, Ms. Gita, Ms. Tian, Ms. Arwa, Ms. Hakyung, Ms. Malwina, Ms. Hayoon, Ms. Yunn, Ms. Esther, Ms. Jin, Mr. Bang, Mr. Janith, Ms. Voni.

I am also grateful to Ms. Nayeon and Ms. Seonyoung who assisted some parts of my experiments.

I am very grateful to Prof. Seok Dockko, Prof. Choi Yongju, Prof. Choe Jongkwon, and Dr. Kim Tschungil for their great comments on my dissertation.

I will forever be grateful to my family and my Vietnamese friends (especially Ms. Le My Chi and Ms. Nguyen Thi Thanh Thao – my flatmates) for their love, kind support, encouragement, and for being with me.

I dedicate this achievement for my all families.